

The *Drosophila* Tumour Suppressor Lgl and Vap33 activate the Hippo pathway by a dual mechanism

Marta Portela^{1,2}, Swastik Mukherjee³, Sayantanee Paul³, John E. La Marca^{1,4,5,6},
Linda M. Parsons^{2,†}, Alexey Veraksa³, Helena E. Richardson^{1,2,7,*}

¹Department of Biochemistry & Chemistry, La Trobe Institute for Molecular Science, La Trobe University, Melbourne, Victoria, 3086, Australia

²Cell Cycle and Development Laboratory, Peter MacCallum Cancer Centre, Melbourne, Victoria, 3002, Australia

³Department of Biology, University of Massachusetts Boston, Boston, MA, 02125, USA

⁴Blood Cells and Blood Cancer Division, Water and Eliza Hall Institute, Melbourne, Victoria, 3052, Australia

⁵Department of Medical Biology, University of Melbourne, Melbourne, Victoria, 3010, Australia

⁶Genome Engineering and Cancer Modelling Program, Olivia Newton-John Cancer Research Institute, Melbourne, Victoria, 3084, Australia

⁷Sir Peter MacCallum Department of Oncology, Department of Anatomy and Neuroscience, Department of Biochemistry and Molecular Biology, University of Melbourne, Melbourne, Victoria, 3010, Australia

*Corresponding author. Email: h.richardson@latrobe.edu.au

†Present address, Faculty of Medicine, University of Tasmania, Hobart, Tasmania, 7005, Australia.

Keywords: *Drosophila*, Lgl, Vap33, Hippo pathway, RtGEF, Git, Arf79F, V-ATPase

Abstract

The tumour suppressor, Lethal (2) giant larvae (Lgl), is an evolutionarily conserved protein that was discovered in the vinegar fly, *Drosophila*, where its depletion results in tissue overgrowth and loss of cell polarity. Lgl links cell polarity and tissue growth through regulation of the Notch and the Hippo signalling pathways. Lgl regulates the Notch pathway by inhibiting V-ATPase activity via Vap33. How Lgl regulates the Hippo pathway was unclear. In this current study, we show that V-ATPase activity inhibits the Hippo pathway, whereas Vap33 acts to activate Hippo signalling. Vap33 physically and genetically interacts with the actin cytoskeletal regulators RtGEF (Pix) and Git, which also bind to Hpo, and are involved in the activation of the Hippo pathway. Additionally, we show that the ADP ribosylation factor Arf79F (Arf1), which is a Hpo interactor, is involved in the inhibition of the Hippo pathway. Altogether our data suggests that Lgl acts via Vap33 to activate the Hippo pathway by a

dual mechanism, 1) through interaction with RtgEF/Git/Arf79F, and 2) through interaction and inhibition of the V-ATPase, thereby controlling epithelial tissue growth.

Introduction

Deregulation of cell polarity and the epithelial-to mesenchymal transition are hallmarks of human cancer (Hanahan and Weinberg, 2011; Muthuswamy and Xue, 2012; Stephens et al., 2018). Key regulators of cell polarity, Lgl, Scribble (Scrib), and Discs large (Dlg), were discovered in *Drosophila* as neoplastic tumour suppressors; these proteins regulate apical-basal cell polarity via their antagonistic interactions with the Par-aPKC and Crb polarity complexes, and also limit cell proliferation (Stephens et al., 2018). Lgl functions to antagonise the activity of aPKC (atypical protein kinase C), and conversely aPKC phosphorylates and inhibits Lgl, in cell polarity regulation and tissue growth control (Stephens et al., 2018). In *Drosophila*, Lgl-aPKC play a role in the control of tissue growth (cell proliferation and survival) that is distinct from their role in cell polarity regulation; *lgl* mutation or aPKC-activation in eye epithelial tissue exhibits increased cell proliferation and survival without loss of apico-basal cell polarity (Grzeschik et al., 2007; Grzeschik et al., 2010). Thus, the Lgl-aPKC axis regulates tissue growth independent of cell polarity effects.

The human Lgl ortholog, LLGL1, has a conserved function with *Drosophila* Lgl, as its expression in *Drosophila* rescues the tumorigenic defects of *lgl* mutants (Grifoni et al., 2004; Grzeschik et al., 2010). Reduced expression or mutations in LLGL1 (HUGL1), are associated with hepatocellular carcinoma (Lu et al., 2009), malignant melanoma (Kuphal et al., 2006) and colorectal cancer (Schimanski et al., 2005). Similarly, aberrant localization or deletion of the second human Lgl homolog, LLGL2 (HUGL2), is associated with gastric epithelial dysplasia and adenocarcinoma (Lisovsky et al., 2009), and with pancreatic intraepithelial neoplasia and ductal adenocarcinoma (Lisovsky et al., 2010). Mislocalization of LLGL1/2 is also observed in other human cancers, including lung adenocarcinoma (Imamura et al., 2013) and ovarian cancer (Grifoni et al., 2007). As occurs in *Drosophila*, the mislocalization/dysfunction of LLGL1/2 in cancer is also associated with altered aPKC localization/activity (Grifoni et al., 2007; Imamura et al., 2013).

We made the novel discovery that in *Drosophila* Lgl acts independent of its apico-basal cell polarity role to regulate the Salvador-Warts-Hippo (Hippo) negative tissue growth control pathway (Grzeschik et al., 2007; Grzeschik et al., 2010). The core of the Hippo pathway involves the serine-threonine protein kinases, Hippo (Hpo) and Warts (Wts), which respond to cell-cell contact and

tissue architectural cues to control tissue growth via phosphorylating the co-transcriptional activator, Yorkie (Yki), which regulates cell proliferation genes (e.g. Cyclin E) and cell survival genes (e.g. Diap1) (Grusche et al., 2010; Richardson and Portela, 2017). Lgl depletion or aPKC activation (which inhibits Lgl) impairs the Hippo pathway via mislocalization of the Hpo protein, away from the apical cortex, where it is normally activated by apical cues (Grzeschik et al., 2010; Parsons et al., 2014a). Thus, Lgl-aPKC controls the Hippo pathway by regulating Hpo localization and activity. In mammalian systems, deregulation of Lgl/aPKC impairs Hippo signalling and induces cell transformation, which mechanistically involves the association of aPKC with the Hpo orthologs, MST1/2, thereby uncoupling MST from the downstream kinase, LATS (Wts) and leading to increased nuclear YAP (Yki) activity (Archibald et al., 2015), consistent with what we observe in *Drosophila* (Grzeschik et al., 2010).

We have also shown that in *Drosophila* Lgl plays a novel regulatory role in ligand-dependent Notch signalling (Parsons et al., 2014b; Portela et al., 2015). Notch activation depends on the cleavage by Adam proteases to produce Notch^{ext}, and then processing by γ -secretase to produce the active form, Notch^{ICD}, which translocates to the nucleus to activate transcription of target genes, such as the *E(spl)* complex, as well as the cell proliferation and survival genes (Ntziachristos et al., 2014). We found that intracellular Notch accumulated in *lgl* mutant tissue, resulting in elevated Notch signalling that contributes to the overgrowth defects in *lgl* mutant tissue (Grzeschik et al., 2010; Parsons et al., 2014b; Portela et al., 2015). In mouse neural development, *Lgl1* knockout exhibits elevated Notch signalling, which is associated with hyperproliferation and differentiation defects (Klezovitch et al., 2004), whilst in zebrafish, *Lgl1* knockdown in the developing retina leads to elevated Notch signalling and neurogenesis defects, which are rescued by blocking Notch activity (Clark et al., 2012).

Intriguingly, we recently found that *lgl* mutant tissue exhibited increased LysoTracker incorporation (Parsons et al., 2014b; Portela et al., 2015), indicating that there is elevated vesicle acidification, due to the activity of the Vacuolar-ATPase (V-ATPase). In the Notch signalling pathway, γ -secretase activity is dependent on vesicle acidification regulated by V-ATPase activity (Kobia et al., 2014; Vaccari et al., 2010). Therefore, in *lgl* mutant tissue the increased V-ATPase activity elevates γ -secretase activity and Notch cleavage, forming Notch^{ICD}, and leading to elevated Notch target gene expression. Consistent with this, genetically or chemically reducing vesicle acidification or V-ATPase function, reduced the elevated Notch signalling in *lgl* mutant tissue (Parsons et al., 2014b; Portela et

al., 2015). Thus, elevated Notch signalling in *lgl* mutant tissue is due to increased vesicle acidification and elevated γ -secretase activity.

To identify novel proteins that link Lgl to the V-ATPase, we undertook affinity purification-mass spectrometry (AP-MS) analysis of Lgl in *Drosophila* S2 tissue culture cells (Portela et al., 2018). Lgl interacted with aPKC and Par6 with high significance as expected. Among the novel interactors of Lgl that bound at high significance, the standout protein involved in endocytosis was the VAMP-(v-SNARE)-associated protein, Vap33, which is an ortholog of human VAPA/VAPB (Portela et al., 2018). Vap33 (VAPA/B) physically and genetically interacts with endocytic regulators and is involved in endo-lysosomal trafficking, with mutations in *Drosophila Vap33* and human *VAPB* resulting in endocytic defects, including the accumulation of the early endosome Rab5 marker (Sanhueza et al., 2015), a phenotype we also observed in *Drosophila lgl* mutant tissue (Parsons et al., 2014b; Portela et al., 2015). We confirmed the binding of Vap33 to Lgl by co-immunoprecipitations (co-IPs) from S2 cells and *in vivo* in *Drosophila* epithelial cells (Portela et al., 2018) by using proximity ligation assays (PLA) (Soderberg et al., 2006). Comparison of our data with the global *Drosophila* proteomics network revealed that Vap33 and Lgl form a network with V-ATPase subunit proteins (Guruharsha et al., 2011; Portela et al., 2018). Interaction with human VAPA/B and V-ATPase proteins was also evident in the human proteome (Huttlin et al., 2015; Portela et al., 2018). We also found that *Vap33* overexpression rescued the elevated Notch signalling in *lgl* mutant eye epithelial clones and the *lgl* mutant adult eye phenotype, whilst knockdown of *Vap33* enhanced these eye defects (Portela et al., 2018). *Vap33* overexpression also reduced V-ATPase activity, as assayed by LysoTracker levels (Petzoldt et al., 2013; Portela et al., 2018). Moreover, in *lgl*-knockdown S2 cells or in *lgl* mutant tissue the interaction between Vap33 and V-ATPase components was decreased (Portela et al., 2018). Thus, Lgl binds to and facilitates the binding of Vap33 to V-ATPase components, which inhibits V-ATPase activity, thereby controlling vesicle acidity, γ -secretase activity and Notch signalling.

Whilst our previous studies have dissected how Lgl regulates the Notch pathway, it is currently not known precisely how Lgl regulates the Hippo pathway. Thus, in this study, we focused on the mechanism of this regulation. We show that the V-ATPase inhibits the Hippo pathway and conversely Vap33 activates the Hippo pathway. Mechanistically, Vap33 is connected to the Hippo pathway by interacting with the cytoskeletal regulators, RtgEF (Pix), Git, and Arf79F (Arf1), which bind to the Hpo protein kinase. Our findings are consistent with a model whereby Lgl-Vap33

promote Hippo signalling via a dual mechanism through interaction with RtGEF-Git-Arf79F and by inhibiting the V-ATPase.

Results

The Hippo signalling pathway is negatively regulated by V-ATPase activity in *Drosophila*.

Our previous studies have revealed the involvement of Lgl in the negative regulation of the V-ATPase (Portela et al., 2018), which is an important regulator of the Notch pathway (Kobia et al., 2014; Vaccari et al., 2010). Since the *lgl* mutant adult eye phenotype (which is due to both Notch and Hippo pathway deregulation) was suppressed by reducing V-ATPase levels (more so than individually inhibiting Notch signalling or reducing Yki/Sd activity (Grzeschik et al., 2010; Parsons et al., 2014b; Portela et al., 2015)), we suspected that the V-ATPase activity might be involved in the regulation of the Hippo pathway. The V-ATPase is comprised of several subunits, and knockdown of any of these proteins reduces V-ATPase function (Collins and Forgac, 2020; Dow, 1999; Dow et al., 1997; Eaton et al., 2021). Indeed, reducing V-ATPase levels/activity using a *Vha68-2* RNAi line resulted in higher Hippo pathway activity as assessed by reduced Yki nuclear staining, and lower expression of the Yki target, *expanded (ex)-lacZ* (**Fig 1B**) compared to the *wild-type* control (**Fig 1A**, quantified in **Fig 1E**). Conversely, knockdown of the core Hippo pathway gene, *wt5*, resulted in impaired Hippo pathway signalling, as assessed by increased Yki nuclear staining and Yki target gene expression (*ex-lacZ*) (**Fig 1C**), and a similar level of pathway impairment was observed upon activating the V-ATPase by overexpressing another V-ATPase subunit *Vha44* (Petzoldt et al., 2013) (**Fig 1D**, quantified in **Fig 1E**), which has been previously shown to elevate V-ATPase activity (Petzoldt et al., 2013). Overexpression of *Vha44* has been previously shown to activate the JNK signalling pathway, however in the eye epithelium JNK activity does not block Hippo signalling but instead is involved in activating Hippo (Doggett et al., 2011; La Marca and Richardson, 2020). Thus, the effect observed upon *Vha44* overexpression on the elevation of the Yki target, *ex-lacZ*, occurs in the background of the elevated JNK-mediated inhibition of Yki activity. From these results we conclude that the V-ATPase negatively regulates the Hippo signalling pathway, leading to the upregulation of Yki activity.

Vap33 activates the Hippo pathway

Since we have previously shown that Lgl functions with Vap33 in negatively regulating the V-ATPase (Portela et al., 2018), we then tested if Vap33 is also involved in Hippo pathway regulation. Here we used the canonical Yki target, *Diap1* (Harvey and Tapon, 2007), to assess Hippo pathway activity.

Whilst Jak-STAT signalling has been shown to induce Diap1 expression in the wing disc during development (Recasens-Alvarez et al., 2017), however expression profiling after activation of the Jak-STAT signalling in the eye epithelium did not identify Diap1 as a target (Flaherty et al., 2009). Additionally, there are no reports that *Lgl* depletion in eye disc clones elevates Jak-STAT signalling (Stephens et al., 2018), but instead loss of cell polarity in mutant clones of the apico-basal polarity gene, *scrib*, in the eye disc results in expression of the Jak-STAT pathway ligand, Upd, and non-cell autonomous induction of Jak-STAT signalling in the surrounding *wild-type* cells (Bunker et al., 2015; Fahey-Lozano et al., 2019; Schroeder et al., 2013). Thus, Diap1 expression is a reliable reporter of Hippo pathway activity in the eye epithelium. As we have previously reported (Grzeschik et al., 2010), in *lgl* mutant clones the levels of the Hippo pathway target, Diap1, were increased (**Fig 2A**, quantified in **Fig 2G**), and a distorted adult eye phenotype was observed (**Fig 2B**). We found that when Vap33 was overexpressed in clones, the expression of Diap1 was reduced (**Fig 2C**, quantified in **Fig 2G**), and adult eyes appeared only slightly disorganised (**Fig 2D**). consistent with Yki activity being reduced. Importantly, overexpression of *Vap33* in *lgl* mutant clones resulted in a reduction of the elevated Diap1 protein levels (**Fig 2E**) that are observed in *lgl* mutant clones (**Fig 2A**) to below *wild-type* levels, similar to *Vap33* overexpression alone (**Fig C**, quantified in **Fig 2G**), and rescued the *lgl* mutant mosaic distorted adult eye phenotype towards that of the *Vap33* overexpressing mosaic adult eye (**Fig 2F** compared with **Fig 2B** and **Fig 2D**), indicating that Vap33 is epistatic to *Lgl*. Together these results show that Vap33 activates the Hippo pathway and that Vap33 is epistatic to *lgl* impairment in the activation of the Hippo pathway.

Vap33 and Lgl form a protein interaction network with RtgEF (Pix), Git, Arf79F and Hpo

Since our results implicated Vap33 in the regulation of the Hippo pathway, we sought to determine whether this occurs via protein-protein interactions. Interestingly, the global human proteomics analysis has elucidated the protein interaction network of the human Vap33 orthologs, VAPA/B, and revealed amongst the interacting proteins the Hpo orthologs, MST1/2 (STK3/4) (Huttlin et al., 2015). To determine whether *Drosophila* Vap33 also interacts with Hpo we conducted affinity purification-mass spectrometry (AP-MS) on endogenously expressed Vap33-YFP *in vivo* using immunoprecipitation with a GFP-nanobody (Neumuller et al., 2012). We decided to use an *in vivo* approach since the common *Drosophila* cell line (S2 cells, thought to be derived from hemocytes) used for protein interaction analysis are not polarised cells, and by using *Drosophila* tissues, we hoped to reveal physiologically relevant interactors important in polarised epithelial tissues. We prepared proteins from Vap33-YFP-expressing embryos and conducted the experiment in triplicate

together with controls. As expected, amongst the AP-MS Vap33 interactors we observed the V-ATPase component, Vha68-2 as a medium confidence interactor (significance analysis of interactome, SAINT score ~0.77) and three other V-ATPase components as lower confidence interactors (**Supp File 1**). Surprisingly, Lgl and Hpo were not detected, suggesting that under the conditions used in embryonic cells these proteins do not form strong interactions with Vap33. However, pertinently, with respect to the Hippo pathway, we detected as high confident interactors (SAINT scores ~1), the Hpo-interacting proteins, RtGEF (Pix, a Rho-type guanine nucleotide exchange factor) and Git (G protein-coupled receptor kinase interacting ArfGAP), are actin cytoskeletal regulators that form a protein complex (Frank and Hansen, 2008; Zhou et al., 2016), and also bind to and activate Hpo (Dent et al., 2015).

To confirm these interactions, we conducted co-immunoprecipitation (co-IP) analyses in S2 cells. We co-transfected Vap33 tagged with V5 and RtGEF tagged with HA and conducted IP-western blot analysis (**Fig 3**). Vap33-V5 co-IPed with RtGEF-HA in both directions (**Fig 3A, B**). We also investigated whether Vap33 and Hpo could form a complex by co-transfecting Vap33-V5 and Hpo-Flag in S2 cells and conducting IP-Western blots. Indeed, Vap33 co-IPed with Hpo in both directions (**Fig 3C, D**). Thus, Vap33 binds to both RtGEF and Hpo, supporting our AP-MS data, and consistent with previous studies showing that Hpo interacts with RtGEF/Git (Dent et al., 2015), and that the human Vap33 orthologs, VAPA/B, interact with the Hpo orthologs STK3/4 (Huttlin et al., 2015).

We then examined whether interactions between Lgl or Vap33 and RtGEF/Git occurred in *Drosophila* larval epithelial tissues, by using the *in situ* proximity ligation assay (PLA) (Soderberg et al., 2006). We have previously used the PLA method to detect robust interactions between Lgl and Vap33 in *Drosophila* epithelial tissue, whilst controls lacking expression of one protein or without one of the antibodies showed minimal positive foci (Portela et al., 2018). First, using larval tissues (eye-antennal epithelial, salivary gland and brain) from endogenously GFP-tagged Lgl flies (Portela et al., 2018; Venken et al., 2011) and antibodies against GFP and Vap33, we confirmed that PLA foci were observed for Lgl and Vap33 (**Fig 4A, Supp Fig 1G, 1H**) (Portela et al., 2018), suggesting that these proteins physically interact *in vivo*. We also observed foci for Lgl-GFP and atypical protein kinase C (aPKC), by using GFP and aPKC antibodies in eye-antennal discs and salivary gland cells (**Supp Fig 1A, C**). Importantly, no PLA signals were observed in the single antibody negative controls (**Supp Fig 1B, 1D-F**). We then conducted PLAs on eye-antennal epithelial and salivary gland tissues using flies expressing the endogenously tagged Lgl-GFP and Git-RFP transgene (Dent et al., 2019), using GFP

and RFP antibodies, which revealed multiple PLA foci (**Fig 4B, Supp Fig 1J**). Likewise, PLAs performed on Git-RFP transgenic fly eye-antennal epithelial and salivary gland tissues using RFP and Vap33 antibodies, revealed multiple PLA foci (**Fig 4C, Supp Fig 1K**). Altogether, the PLA data confirmed that Git interacts *in vivo* with Vap33 and Lgl in the *Drosophila* larval eye-antennal epithelium (**Fig 4**), as well as other polarised cells in the salivary gland and brain (**Supp Fig 1**).

Interestingly, in mammalian cells, Git interacts with the ADP ribosylation factor, Arf1 and inhibits its activity (Zhou et al., 2016), and examination of the *Drosophila* Hippo pathway proteomics dataset (Kwon et al., 2013), revealed that the *Drosophila* Arf1 ortholog, Arf79F, is a high confidence interactor with Hpo (SAINT score >0.8), which was validated by co-IP analysis (Kwon et al., 2013). Based on these physical interactions, we also tested by PLA whether Arf79F interacted with Git, RtGEF and Hpo. Indeed, using flies containing a Hpo-GFP-Venus transgene (Pojer et al., 2021) and antibodies against Arf79F, we confirmed via PLA that Hpo and Arf79F interact in eye-antennal epithelial and brain tissue (**Fig 4D, Supp Fig 1I**). Similarly, using PLAs on eye-antennal discs and salivary glands from Git-RFP or RtGEF-RFP transgenic flies (Dent et al., 2019) and RFP and Arf79F antibodies, Arf79F was confirmed to interact with Git and RtGEF (**Fig 4E, 4F, Supp Fig 1L, M**). Thus, we have revealed that Arf79F binds to Git, RtGEF and Hpo in eye-antennal tissue (**Fig 4**), as well as salivary gland or brain tissues (**Supp Fig 1**). The lower levels of PLA signals in some samples may be due to low levels of expression of the proteins or lower levels of protein-protein interactions.

Vap33 overexpression rescues increased Hippo pathway target gene expression in *RtGEF* mutant tissue

To determine if *Vap33* genetically interacts with *RtGEF*, we examined the expression of the Hippo pathway target, Diap1, in *RtGEF* mutant (*RtGEF^{P1036}*) clones that overexpress Vap33. Individually, *RtGEF* mutant clones showed increased Diap1 expression (**Fig 5A**), as expected (Dent et al., 2015), and resulted in a slightly enlarged adult eye phenotype (**Fig 5B**). The elevated Diap1 expression observed in *RtGEF* mutant clones was rescued to normal levels upon *Vap33* overexpression (**Fig 5C**, quantified in **Fig 5E**), and the adult eye size was normalized (**Fig 5D**). Thus, consistent with the protein interactions, RtGEF and Vap33 genetically interact in the regulation of the Hippo pathway in a manner consistent with both Vap33 and RtGEF acting to induce Hippo pathway activity.

Git knockdown rescues the reduced Hippo pathway target gene expression in *Vha68-2* mutant clones

Next, we examined genetic interactions between Git and a component of the V-ATPase, *Vha68-2*, in Hippo pathway regulation. Previous analysis of Git/RtGEF knockdown tissue reveals that Yki targets are upregulated, however the adult mosaic eyes were similar to the *wild-type* control (Dent et al., 2015) (data not shown). As we have previously observed, *Vha68-2* mutant clones were small although they did not show indications of cell death and were retained into pupal development (Portela et al., 2018). Consistent with our analysis of, *ex-lacZ* (Fig 1C), *Vha68-2* mutant clones also showed reduced expression of the Hippo pathway target, Diap1 (Fig 6C) relative to *wild-type* clones (Fig 6A, quantified in Fig 6G), and resulted in reduced and disorganised adult eyes relative to the *wild-type* control (Fig 6D compared with Fig 6B). When Git was knocked down using a transgenic RNAi line in *Vha68-2* mutant clones, partial rescue of the reduced Diap1 expression was observed (Fig 6E, quantified in Fig 6G) and the disorganised *Vha68-2* mutant mosaic adult eye phenotype was strongly rescued to be similar to *wild-type* adult eyes (Fig 6F compared with Fig 6D and Fig 6B). These results show that the reduced Yki activity (low Diap1 expression) that occurs in *Vha68-2* mutant clones is rescued by Git1 knockdown, and suggests that the activation of Hippo signalling (reduced Diap1 expression) that occurs upon reducing V-ATPase activity depends upon Git. A possible interpretation for this genetic interaction is that V-ATPase activity may oppose the action of Git1/RtGEF to activate Hpo.

Arf79F is required for Lgl-mediated regulation of the Hippo pathway

We then tested whether Arf79F is required for the regulation of the Hippo pathway by Lgl. As we previously observed, *lgl* mutant tissue shows impaired Hippo pathway signalling, as revealed by the elevated levels of Diap1 (Fig 7C compared to the control, Fig 7A, quantified in Fig 7M) and results in a distorted, disorganised adult eye phenotype relative to the *wild-type* control (Fig 7D compared with Fig 7B). We therefore sought to determine whether *Arf79F* genetically interacts with *lgl* in its regulation of the Hippo pathway. When *Arf79F* was knocked down, using a RNAi line (which we showed effectively reduced Arf79F protein levels in eye disc clones, Supp Fig 2A, B), a decrease in Diap1 expression was observed and clones were smaller than *wild-type* clones (Fig 7E), suggesting that the *Arf79F* knockdown clones have reduced tissue growth, consistent with Hippo pathway upregulation. However, the *Arf79F* adult mosaic eyes showed only slight disorganisation (Fig 7F relative to the wild-type control, Fig 7B). Knockdown of *Arf79F* in *lgl* mutant clones also resulted in low Diap1 levels, similar to *Arf79F* knockdown alone (Fig 7G compared with Fig 7E, quantified in Fig

7M), suggesting that *Arf79F* is epistatic to *lgl* in the regulation of the Hippo pathway. Consistent with this, the *lgl* mutant mosaic distorted adult eye phenotype was normalised upon *Arf79F* knockdown (**Fig 7H** compared with **Fig 7D** and **Fig 7B**). Additionally, we used a dominant-negative version of the activator of *Arf79F*, *Sec71* (*Sec71^{DN}*), to reduce *Arf79F* function. When expressed individually in clones, *Sec71^{DN}* had no significant effect upon *Diap1* levels (**Fig 7I**, quantified in **Fig 7M**), and did not obviously affect the adult eye phenotype (**Fig 7J**). However, when *Sec71^{DN}* was expressed in *lgl* mutant clones, lower *Diap1* levels were observed (**Fig 7K**, quantified in **Fig 7M**), and the *lgl* mutant mosaic adult eye phenotype was normalised toward wild-type (**Fig 7L** compared with **Fig 7D** and **Fig 7B**). Interestingly, although *Sec71^{DN}* expression did not have a significant effect on *Diap1* expression on its own, when expressed in *lgl* mutant clones it reduced *Diap1* levels to below that of the control (**Fig 7M**), suggesting that *Lgl* depletion depends on *Sec71* (and thus *Arf79F*) to inhibit Hippo signalling. These results show that, consistent with the binding of *Arf79F* with *Hpo* (**Fig 4D**), knockdown of *Arf79F* reduces *Diap1* expression, suggesting that *Arf79F* acts to inhibit the Hippo pathway. Furthermore, knockdown of *Arf79F* (or expression of *Sec71^{DN}*) rescued the elevated expression of *Diap1* in *lgl* mutant clones (**Fig 7M**), indicating that *Arf79F* levels/activity are required for the inhibition of Hippo signalling in *lgl* mutant tissue. Thus, *Arf79F* is a negative regulator of Hippo signalling that acts downstream of *Lgl*. Since mammalian *Git* proteins act to inhibit *Arf1* activity (Zhou et al., 2016), our results are consistent with a mechanism where *Lgl* and *Vap33* promote *RtGEF*/*Git* activity to inhibit *Arf79F* (*Arf1*), and thereby activate the Hippo pathway.

Discussion

In this study we have revealed a new mechanism for the control of the Hippo pathway by the cell polarity regulator, *Lgl*. We show herein that V-ATPase activity leads to inhibition of Hippo signalling, and conversely that *Vap33* activates the Hippo pathway downstream of *Lgl*. We discovered that *Vap33* physically interacts with *RtGEF* and *Git* using *in vivo* affinity-purification mass spectrometry. *RtGEF* and *Git* are *Hpo* interactors (Dent et al., 2019), and we confirmed that *Vap33* interacts with *RtGEF* and *Hpo* in S2 cells, and that *Vap33* and *Lgl* are in close proximity with *Git* in *Drosophila* cells. We also show that the ADP ribosylation factor, *Arf79F*, the mammalian ortholog of which (*ARF1*) binds to the mammalian *Git* orthologs, *GIT1/2* (Zhou et al., 2016), and is in close proximity with *Git*, *RtGEF* and *Hpo* in *Drosophila* cells. Functionally, we show that overexpression of *Vap33* rescues the elevated *Diap1* levels (impaired Hippo signalling) in *RtGEF* mutant clones. Furthermore, the reduced *Diap1* expression (elevated Hippo signalling) upon V-ATPase impairment (*Vha68-2* mutant clones) is rescued by knockdown of *Git*. We also show that *Arf79F* knockdown leads to reduced *Diap1*

expression (increased Hippo signalling) downstream of Lgl. Altogether, our data are consistent with a model where Lgl and Vap33 activate the Hippo pathway by a dual mechanism: 1) Lgl and Vap33, through interaction with RtGEF/Git/Arf79F, positively regulate Hippo pathway activity, and 2) Lgl and Vap33, through interaction with components of the V-ATPase, block V-ATPase activation and prevent its negative regulation of the Hippo pathway (**Fig 8**). Precisely how the V-ATPase functions to regulate Hippo signalling is unknown. However, the V-ATPase acts to increasing vesicle acidification, and this has been shown to impact the efficacy of many signalling pathways (Collins and Forgac, 2020; Eaton et al., 2021; Pamarthi et al., 2018). The V-ATPase might therefore act to inhibit Hippo pathway signalling by blocking the interaction of Lgl/Vap33/RtGEF/Git/Arf79F with Hpo on endosomes, thereby altering Hpo localization and inhibiting its activity. Consistent with this notion, we observed that Lgl colocalizes with endocytic vesicle markers (Parsons et al., 2014b), and that Hpo localization is altered in *lgl* mutant tissue (Grzeschik et al., 2010). Furthermore, Hpo signalling is associated with endosomal regulators (Verghese and Moberg, 2019), and the subcellular localization of Hpo has been shown to be important for its activation, and for Hpo-mediated phosphorylation and activation of its downstream protein kinase, Wts (Sun et al., 2015).

In their interactions with the Hippo pathway, Git and RtGEF function to activate Hpo (Dent et al., 2015), while our analyses indicate that Arf79F acts to inhibit Hippo signalling, since elevated Hippo pathway activity (increased Diap1 expression) in *lgl* mutant clones was normalised upon knockdown or inhibition of Arf79F. Previous studies examining the interactions between mammalian orthologues of Git and Arf79F, showed that GIT1/2 acts to inactivate ARF1 (Zhou et al., 2016), and therefore it is likely that Git (and RtGEF) act to block Arf79F activity to mediate Hpo activation (**Fig 8**). Lgl and Vap33 might then function to promote Git/RtGEF inhibition of Arf79F, facilitating activation of Hpo. Arf79F (ARF1) is a regulator of vesicular trafficking (Adarska et al., 2021), and may inhibit Hpo by relocalizing it away from its activators, such as Expanded and Fat, at specific apical subcellular domains (Sun et al., 2015). Interestingly, from our previous Lgl interactome analysis, Arf79F can be linked to Lgl through the Arf79F-binding protein Rab5 (Guruharsha et al., 2011; Kwon et al., 2013), which also binds to Lgl and aPKC at high confidence, SAINT score ~1) ((Portela et al., 2018) and unpublished data). Thus, it is possible that the early endosomal regulator, Rab5, may also be involved in linking Lgl/Vap33 and aPKC to Arf79F in early endosomes, where they may also interact with Vap33, Git/RtGEF and Hpo.

It is unclear whether the RtGEF/Git regulated protein kinase, Pak (Zhou et al., 2016), is involved in the regulation of Hippo signalling, since although individual knockdown of two Pak paralogs in *Drosophila*, Pak1 and Pak3, did not affect Hippo pathway signalling (Dent et al., 2015), it is possible that there may be redundancy between Pak1, Pak3, and the third *Drosophila* Pak paralog, Mushroom bodies tiny (Mbt) (Melzer et al., 2013; Menzel et al., 2008; Menzel et al., 2007; Schneeberger and Raabe, 2003), in the regulation of Hippo pathway signalling. Pak proteins have been shown to be involved in cell polarity, F-actin regulation and morphogenesis in *Drosophila* (Asano et al., 2009; Baek et al., 2012; Bahri et al., 2010; Conder et al., 2007; Felix et al., 2015; Harden et al., 1996; Menzel et al., 2008; Menzel et al., 2007; Schneeberger and Raabe, 2003; Vlachos and Harden, 2011), however Mbt also plays a role in tissue growth during *Drosophila* development (Lim et al., 2019; Melzer et al., 2013), suggesting Mbt is a candidate for investigation of a potential role downstream of RtGEF/Git in Hippo pathway regulation.

Our analyses here, and in our previous study (Portela et al., 2018), have revealed that Lgl interacts with Vap33 to positively regulate the Hippo pathway and to negatively regulate the Notch pathway. Mechanistically, Lgl/Vap33 inhibits the Notch pathway by inhibiting V-ATPase activity and reducing vesicle acidification that is required for the cleavage of the Notch receptor and release of Notch^{ICD} from vesicles (Portela et al., 2018), where it can then translocate into the nucleus and promote transcription of its target genes (**Fig 8**). Interestingly, Arf79F (Arf1) is required for Notch signalling in *Drosophila* hemocyte differentiation, where it promotes Notch trafficking (Khadilkar et al., 2014). Thus, it is possible that Lgl/Vap33/RtGEF/Git may also inhibit Arf79F to reduce Notch signalling, and that in *lgl* mutant tissue elevated Arf79F activity may also contribute to the elevated Notch activation. Indeed, we found that Arf79F is required for the elevated Notch pathway signalling in *lgl* mutant clones, since *Arf79F* knockdown in *lgl* mutant clones normalized the expression of the Notch pathway reporter, *E(spl)m8-lacZ* (**Supp Fig 3**). Whether RtGEF/Git are also regulators of Notch signalling remains to be determined.

In summary, our study has revealed a new mechanism for Hippo pathway regulation by the cell polarity and tumour suppressor protein, Lgl. Mechanistically, Lgl and Vap33 function in a dual manner to promote Hippo signalling by both reducing V-ATPase activity, and thereby preventing V-ATPase from inhibiting Hippo signalling and by acting through RtGEF/Git to prevent Arf79F from inhibiting Hpo. By promoting Hippo signalling as well as inhibiting Notch signalling, Lgl/Vap33 function to limit tissue growth. Mutation of Lgl therefore results in tissue overgrowth due to

inhibition of the Hippo pathway and activation of the Notch pathway. However, despite the dual regulation of Hippo and Notch signalling by Lgl and Vap33, the *lgl* mutant phenotype doesn't completely mirror the *Vap33* mutant phenotype (Portela et al., 2018), which is likely due to Vap33 having additional roles in vesicle trafficking, proteolysis and signalling (Borgese et al., 2021; Choi et al., 2012; Deivasigamani et al., 2014; Gao et al., 2023; Mao et al., 2019; Sanhueza et al., 2015; Tsuda et al., 2008), and Lgl having additional roles in cell polarity regulation (Grifoni et al., 2013; Stephens et al., 2018). The dual mechanism of Notch and Hippo pathway regulation by Lgl/Vap33 may be important in limiting tissue growth during development and may play a role in tissue homeostasis, enabling cell proliferation to occur after tissue damage, thereby enabling wound repair. Indeed, Hippo pathway signalling is inhibited, and Notch pathway signalling is activated after tissue wounding and both pathways are involved in tissue regeneration (Blanco et al., 2010; Chen et al., 2012; Grusche et al., 2011; Kux and Pitsouli, 2014). However, the involvement of Lgl/Vap33/Git/RtGEF/Arf79F and the V-ATPase in the regulation of Hippo and Notch signalling during the response to tissue wounding remains to be determined. Furthermore, whether the mammalian orthologs of Lgl and Vap33 also act via these mechanisms to control tissue growth in mammals remains to be determined.

Experimental Procedures

Drosophila stocks and husbandry

Fly stocks were generated in house or obtained from other laboratories or stocks centers as detailed in **Table S1**. All *Drosophila* genotypes for all the samples analysed in the figures and detailed in **Table S2**. All fly stocks and crosses were raised and undertaken on a standard cornmeal/molasses/yeast medium within temperature-controlled incubators at 25°C.

Clonal Analysis

Mosaic analysis with a repressible cell marker (MARCM (GFP+)) (Lee and Luo, 2001) clones were generated as previously described (Grzeschik et al., 2010), using the following stock: *ey-FLP, UAS-GFP; Tub-GAL80, FRT40A; Tub-GAL4/TM6B* MARCM 2L. Crosses were set up and left overnight at room temperature. Adults were then turned daily into new vials and allowed to lay for ~24 hours at 25°C. L3 animals were then collected after ~144 hours (6 days after the egg laying period). Samples were collected and prepared as described across multiple days to be similarly aged, and then stored at 4°C in 80% glycerol as necessary prior to mounting.

Heat shock induced Flip-out clones were generated using the stock: *hs-FLP; ex-lacZ; Act>CD2>GAL4, UAS-GFP*. Specifically, clones were induced by heat shocking larvae at 37°C for 15 minutes roughly 72 hours after egg laying. L3 imaginal discs were then dissected and prepared as described 72h after clone induction.

Immunofluorescence

Third-instar larval eye-antennal discs, were dissected in phosphate-buffered saline (PBS), fixed in 4% paraformaldehyde for 30min, washed in PBS + 0.1 or 0.3% Triton X-100 (PBT), and blocked in PBT + 1% BSA (PBT/BSA). The tissues were incubated with the primary antibody in PBT/BSA over night at 4°C. After washing off the primary antibodies the tissues were incubated with the secondary antibodies in PBT for 1h at room temperature. After washing off the secondary antibodies the samples were mounted in 80% glycerol or Vectashield (Vector Laboratories).

Antibodies used were; mouse β -galactosidase (Sigma, 1:500), rabbit GFP (Invitrogen A11122, 1:500), mouse GFP (Invitrogen A11120, 1:500); mouse RFP (Invitrogen RF5R, 1:100) rabbit Yki (gift from K. Irvine, 1:400), mouse Diap1 (gift from B. Hay, 1:100), rabbit Vap33 (gift from H. Bellen, 1:1000), rabbit aPKC (Santa Cruz, 1:1000), rabbit Arf79F (gift from M.S. Inamdar, 1:500 (Khadilkar et al., 2014)). Guinea pig Arf79F (gift from F. Yu, 1:200 (Wang et al., 2017)).

Secondary antibodies used were; anti-mouse Alexa 568, 633, 647, anti-rabbit Alexa 568, 633, and anti-guinea pig Alexa 568, 633 (1:500). DNA was stained with 2-(4-amidinophenyl)-1H-indole-6-carboxamide (DAPI, 1 μ M).

Affinity Purification-Mass Spectrometry

Flies expressing endogenously YFP-tagged Vap33 (line #115288, Kyoto Stock Center) were grown in population cages, with embryos laid overnight collected on apple juice/agar plates. Extraction and protein purification were carried out as described in Neumuller et al. (Neumuller et al., 2012). Briefly, extracts were prepared using Default Lysis Buffer (DLB) (50 mM Tris pH 7.5, 125 mM NaCl, 5% glycerol, 0.2% IGEPAL, 1.5 mM MgCl₂, 1 mM DTT, 25 mM NaF, 1mM Na₃VO₄, 1mM EDTA, and 2x Complete protease inhibitor, Roche), spun down to clarify, incubated first with empty agarose beads and then with GFP-Trap resin (ChromoTek), followed by washes and elution in SDS sample buffer.

The eluates were loaded on SDS-polyacrylamide gel and electrophoresed so that the dye front migrated ~1 cm in the separating gel. The gel was then stained with Coomassie blue, and the lane was cut into two 5 mm x 5 mm pieces and sent for mass spectrometry analysis (Taplin Mass Spectrometry Facility, Harvard Medical School). Samples were digested with trypsin in-gel and peptides were analyzed using a Thermo Scientific Orbitrap mass spectrometer. The mass spectrometry analysis was conducted on three biological replicates for both experimental samples (*Vap33-YFP*) and controls (*yw* fly line). Data were analysed using the Significance Analysis of Interactome (SAINT) program (Choi et al., 2011), and a complete table of Vap33-YFP-interacting proteins is included as **Supplemental File 1**. Mass spectrometry data were deposited to the ProteomeXchange Consortium via the PRIDE partner repository (Perez-Riverol et al., 2022) with the data set identifier PXD035110.

Co-immunoprecipitation (co-IP) and Western Blot Analysis

Constructs used were: pMT-Vap33-V5 (Portela et al., 2018), pAc5.1-Flag-Hpo (Dent et al., 2015) and pAC5-1-HA-RtGEF (Dent et al., 2015). *Drosophila* S2 cells were maintained in standard Schneider's S2 medium with fetal bovine serum (Gibco) at 25°C, and transfections were performed using Effectene transfection reagent (Qiagen). CuSO₄ was added to culture media at a final concentration of 0.35 mM for inducing expression of Vap33-HA. Cells were lysed using DLB (see above) and spun down to remove debris. Clear cell lysates were incubated with anti-V5, anti-HA, or anti-Flag beads (Sigma) for 2 hrs at 4°C. Beads were washed three times with lysis buffer, and protein complexes were eluted with SDS buffer. Proteins were separated via SDS-PAGE, blotted, incubated with primary and secondary antibodies, and signal was detected using the Odyssey imaging system (LI-COR). Primary antibodies used were: mouse anti-V5 (Sigma, 1:1,000), rabbit anti-Flag (Sigma, 1:1,000), rabbit anti-HA (Sigma, 1:1,000). Secondary antibodies used were: IRDye 800CW Donkey anti-Rabbit IgG (LI-COR), IRDye 680CW Donkey anti-Mouse IgG (LI-COR).

Proximity ligation assay

The interactions between Lgl and aPKC, Vap33 or Git; Arf79F and Git, RtGEF or Hpo; and Vap33 and Git in *Drosophila* larval tissues were detected *in situ* using the Duolink® In Situ Red Starter Kit Mouse/Rabbit (Sigma, DUO92101) according to the instructions of the manufacturer. Briefly, primary antibody incubation was applied using the same conditions as immune-histofluorescence staining. Duolink secondary antibodies against the primary antibodies were then added. These

secondary antibodies were provided as conjugates to oligonucleotides that were able to form a closed circle through base pairing and ligation using Duolink ligation solution when the antibodies were in close proximity (Soderberg et al., 2006) (a distance estimated to be <40 nm (Koos et al., 2014)). The detection of the signals was conducted by rolling circle amplification using DNA polymerase incorporating fluorescently labelled nucleotides into the amplification products. The resulting positive signals were visualized as bright fluorescent dots, with each dot representing one interaction event. As technical negative control one of the primary antibodies was not added therefore, no positive signals were obtained from that assay. An additional negative control was performed in a tissue without one of the antigens (GFP) and the full protocol was performed in those tissues. As a positive control, antibodies against two well-known interactors in the tissues, Lgl-aPKC and Lgl-Vap33, were used. The tissues were visualized using confocal microscopy (Zeiss Confocal LSM 780 PicoQuant FLIM or Zeiss LSM 800 Airyscan laser scanning confocal).

Primary antibody pairs used were mouse GFP with rabbit Vap33 (**Fig. 4A, S1G, H**), mouse RFP with rabbit GFP (**Fig. 4B, S1J**), mouse RFP with rabbit Vap33 (**Fig. 4C, S1K**), mouse GFP with rabbit Arf79F (**Fig. 4D, S1I**), mouse RFP with rabbit Arf79F (**Fig. 4E, F, S1L, M**), mouse GFP with rabbit aPKC (**Fig. S1A, C**). A GFP-tagged version of Lgl was used to detect interactions with Vap33, since the Lgl and Vap33 antibodies were both raised in rabbit. GFP-tagged Hpo was also used since the available Hpo antibody was raised in rats, and PLA antibodies designed for use with rat-raised antibodies were unavailable. RFP-tagged versions of RtGEF and Git were used for similar reasons.

Imaging

Fluorescent-labelled samples were mounted in 80% glycerol or Vectashield (Vector Laboratories) and analysed by confocal microscopy (LEICA TCS SP5, Zeiss Confocal LSM 780 PicoQuant FLIM or Zeiss LSM 800 Airyscan laser scanning confocal). Images were processed using Leica LAS AF Lite and Fiji (Image J 1.50e). Images were assembled using Photoshop 21.2.3 (Adobe). Adult eyes were imaged on a dissecting microscope using a Scitec Infinity1 camera. Images were processed, analysed, and assembled using some combination of LAS AF Lite (Leica), Zen 2012 (Zeiss), Fiji and Photoshop 21.2.3 (Adobe).

Statistical Analysis of Signal Intensity

Relative *Ex-lacZ* (Fig. 1), or *E(spl)m8-lacZ* (Fig. S3) β Gal stainings, and Diap1 stainings (Fig. 2, 5, 6, 7)) within eye discs was determined using images taken at the same confocal settings. Average pixel intensity was measured using the measurement log tool from Fiji or Photoshop 5.1 (Adobe). In the case of *E(spl)m8-lacZ* analyses, clones were chosen just posterior to the morphogenetic furrow of each eye disc. Average pixel intensity was measured in mutant clones and the *wild-type* adjacent tissue of the same areas and expressed as a ratio of pixel intensity of the mutant clone relative to the *wild-type* tissue. To analyze and plot data, we used Microsoft Excel 2013 and GraphPad Prism 9. We performed a D'Agostino and Pearson normality test, and the data found to have a normal distribution were analysed by a two-tailed t test with Welch correction. In the case of multiple comparisons, we used a one-way ANOVA with Bonferroni post-test. Error bars represent SEM.

Acknowledgments

We are grateful to all those who contributed fly stocks or antibodies to this study, to Bloomington, VDRC and NIG Stock Centers, OzDros and Flybase. HER was supported by a Senior Research Fellowship from the National Health and Medical Research Council (NHMRC) Australia, and funds from La Trobe University and La Trobe School of Molecular Science. This work was supported by grants from the NHMRC (APP1160025) to HER and AV, the Cancer Council Victoria Australia (APP1041817) to HER and AV, and the CASS (Contributing to Australian Scholarship and Science) Foundation (SM/13/4847) to LMP, and a National Institute of Health grant GM123136 to AV.

Author contributions

HER, AV, MP designed the study, MP, LMP, SM, SP, JELM conducted experiments, MP, SM prepared figures, HER, MP wrote the paper, and JELM, AV provided editorial guidance.

Competing Interests: The authors declare that they have no conflicts of interest, and no financial and non-financial competing interests.

References

- Adarska, P., Wong-Dilworth, L. and Bottanelli, F.** (2021). ARF GTPases and Their Ubiquitous Role in Intracellular Trafficking Beyond the Golgi. *Front Cell Dev Biol* **9**, 679046.
- Archibald, A., Al-Masri, M., Liew-Spilger, A. and McCaffrey, L.** (2015). Atypical protein kinase C induces cell transformation by disrupting Hippo/Yap signaling. *Mol Biol Cell* **26**, 3578-95.
- Asano, Y., Jimenez-Dalmaroni, A., Liverpool, T. B., Marchetti, M. C., Giomi, L., Kiger, A., Duke, T. and Baum, B.** (2009). Pak3 inhibits local actin filament formation to regulate global cell polarity. *HFSP J* **3**, 194-203.
- Baek, S. H., Cho, H. W., Kwon, Y. C., Lee, J. H., Kim, M. J., Lee, H. and Choe, K. M.** (2012). Requirement for Pak3 in Rac1-induced organization of actin and myosin during Drosophila larval wound healing. *FEBS Lett* **586**, 772-7.
- Bahri, S., Wang, S., Conder, R., Choy, J., Vlachos, S., Dong, K., Merino, C., Sigrist, S., Molnar, C., Yang, X. et al.** (2010). The leading edge during dorsal closure as a model for epithelial plasticity: Pak is required for recruitment of the Scribble complex and septate junction formation. *Development* **137**, 2023-32.
- Blanco, E., Ruiz-Romero, M., Beltran, S., Bosch, M., Punset, A., Serras, F. and Corominas, M.** (2010). Gene expression following induction of regeneration in Drosophila wing imaginal discs. Expression profile of regenerating wing discs. *BMC Dev Biol* **10**, 94.
- Borgese, N., Iacomino, N., Colombo, S. F. and Navone, F.** (2021). The Link between VAPB Loss of Function and Amyotrophic Lateral Sclerosis. *Cells* **10**.
- Bunker, B. D., Nellimoottil, T. T., Boileau, R. M., Classen, A. K. and Bilder, D.** (2015). The transcriptional response to tumorigenic polarity loss in Drosophila. *Elife* **4**.
- Chen, L., Qin, F., Deng, X., Avruch, J. and Zhou, D.** (2012). Hippo pathway in intestinal homeostasis and tumorigenesis. *Protein Cell* **3**, 305-10.
- Choi, H., Larsen, B., Lin, Z. Y., Breitkreutz, A., Mellacheruvu, D., Fermin, D., Qin, Z. S., Tyers, M., Gingras, A. C. and Nesvizhskii, A. I.** (2011). SAINT: probabilistic scoring of affinity purification-mass spectrometry data. *Nat Methods* **8**, 70-3.
- Choi, S. W., Yeon, J. T., Park, K. I., Lee, C. H., Youn, B. S., Oh, J. and Lee, M. S.** (2012). VapB as a regulator of osteoclastogenesis via modulation of PLCgamma2-Ca(2+)-NFAT signaling. *FEBS Lett* **586**, 263-9.

Clark, B. S., Cui, S., Miesfeld, J. B., Klezovitch, O., Vasioukhin, V. and Link, B. A. (2012). Loss of Lgl1 in retinal neuroepithelia reveals links between apical domain size, Notch activity and neurogenesis. *Development* **139**, 1599-610.

Collins, M. P. and Forgac, M. (2020). Regulation and function of V-ATPases in physiology and disease. *Biochimica Et Biophysica Acta-Biomembranes* **1862**.

Conder, R., Yu, H., Zahedi, B. and Harden, N. (2007). The serine/threonine kinase dPak is required for polarized assembly of F-actin bundles and apical-basal polarity in the Drosophila follicular epithelium. *Dev Biol* **305**, 470-82.

Deivasigamani, S., Verma, H. K., Ueda, R., Ratnaparkhi, A. and Ratnaparkhi, G. S. (2014). A genetic screen identifies Tor as an interactor of VAPB in a Drosophila model of amyotrophic lateral sclerosis. *Biol Open* **3**, 1127-38.

Dent, L. G., Manning, S. A., Kroeger, B., Williams, A. M., Saiful Hilmi, A. J., Crea, L., Kondo, S., Horne-Badovinac, S. and Harvey, K. F. (2019). The dPix-Git complex is essential to coordinate epithelial morphogenesis and regulate myosin during Drosophila egg chamber development. *PLoS Genet* **15**, e1008083.

Dent, L. G., Poon, C. L., Zhang, X., Degoutin, J. L., Tipping, M., Veraksa, A. and Harvey, K. F. (2015). The GTPase regulatory proteins Pix and Git control tissue growth via the Hippo pathway. *Curr Biol* **25**, 124-30.

Doggett, K., Grusche, F. A., Richardson, H. E. and Brumby, A. M. (2011). Loss of the Drosophila cell polarity regulator Scribbled promotes epithelial tissue overgrowth and cooperation with oncogenic Ras-Raf through impaired Hippo pathway signaling. *BMC Dev Biol* **11**, 57.

Dow, J. A. (1999). The multifunctional Drosophila melanogaster V-ATPase is encoded by a multigene family. *J Bioenerg Biomembr* **31**, 75-83.

Dow, J. A., Davies, S. A., Guo, Y., Graham, S., Finbow, M. E. and Kaiser, K. (1997). Molecular genetic analysis of V-ATPase function in Drosophila melanogaster. *J Exp Biol* **200**, 237-45.

Eaton, A. F., Merkulova, M. and Brown, D. (2021). The H⁺-ATPase (V-ATPase): from proton pump to signaling complex in health and disease. *American Journal of Physiology-Cell Physiology* **320**, C392-C414.

Fahey-Lozano, N., La Marca, J. E., Portela, M. and Richardson, H. E. (2019). Drosophila Models of Cell Polarity and Cell Competition in Tumourigenesis. *Adv Exp Med Biol* **1167**, 37-64.

Felix, M., Chayengia, M., Ghosh, R., Sharma, A. and Prasad, M. (2015). Pak3 regulates apical-basal polarity in migrating border cells during *Drosophila* oogenesis. *Development* **142**, 3692-703.

Flaherty, M. S., Zavadil, J., Ekas, L. A. and Bach, E. A. (2009). Genome-wide expression profiling in the *Drosophila* eye reveals unexpected repression of notch signaling by the JAK/STAT pathway. *Dev Dyn* **238**, 2235-53.

Frank, S. R. and Hansen, S. H. (2008). The PIX-GIT complex: a G protein signaling cassette in control of cell shape. *Semin Cell Dev Biol* **19**, 234-44.

Gao, X. K., Sheng, Z. K., Lu, Y. H., Sun, Y. T., Rao, X. S., Shi, L. J., Cong, X. X., Chen, X., Wu, H. B., Huang, M. et al. (2023). VAPB-mediated ER-targeting stabilizes IRS-1 signalosomes to regulate insulin/IGF signaling. *Cell Discov* **9**, 83.

Grifoni, D., Froidi, F. and Pession, A. (2013). Connecting epithelial polarity, proliferation and cancer in *Drosophila*: the many faces of Lgl loss of function. *Int J Dev Biol* **57**, 677-87.

Grifoni, D., Garoia, F., Bellosta, P., Parisi, F., De Biase, D., Collina, G., Strand, D., Cavicchi, S. and Pession, A. (2007). aPKCzeta cortical loading is associated with Lgl cytoplasmic release and tumor growth in *Drosophila* and human epithelia. *Oncogene* **26**, 5960-5.

Grifoni, D., Garoia, F., Schimanski, C. C., Schmitz, G., Laurenti, E., Galle, P. R., Pession, A., Cavicchi, S. and Strand, D. (2004). The human protein Hugl-1 substitutes for *Drosophila* lethal giant larvae tumour suppressor function in vivo. *Oncogene* **23**, 8688-94.

Grusche, F. A., Degoutin, J. L., Richardson, H. E. and Harvey, K. F. (2011). The Salvador/Warts/Hippo pathway controls regenerative tissue growth in *Drosophila melanogaster*. *Dev Biol* **350**, 255-66.

Grusche, F. A., Richardson, H. E. and Harvey, K. F. (2010). Upstream regulation of the hippo size control pathway. *Curr Biol* **20**, R574-82.

Grzeschik, N. A., Amin, N., Secombe, J., Brumby, A. M. and Richardson, H. E. (2007). Abnormalities in cell proliferation and apico-basal cell polarity are separable in *Drosophila* Lgl mutant clones in the developing eye. *Dev Biol* **311**, 106-23.

Grzeschik, N. A., Parsons, L. M., Allott, M. L., Harvey, K. F. and Richardson, H. E. (2010). Lgl, aPKC, and Crumbs regulate the Salvador/Warts/Hippo pathway through two distinct mechanisms. *Curr Biol* **20**, 573-81.

Guruharsha, K. G., Rual, J. F., Zhai, B., Mintseris, J., Vaidya, P., Vaidya, N., Beekman, C., Wong, C., Rhee, D. Y., Cenaj, O. et al. (2011). A protein complex network of *Drosophila melanogaster*. *Cell* **147**, 690-703.

Hanahan, D. and Weinberg, R. A. (2011). Hallmarks of cancer: the next generation. *Cell* **144**, 646-74.

Harden, N., Lee, J., Loh, H. Y., Ong, Y. M., Tan, I., Leung, T., Manser, E. and Lim, L. (1996). A *Drosophila* homolog of the Rac- and Cdc42-activated serine/threonine kinase PAK is a potential focal adhesion and focal complex protein that colocalizes with dynamic actin structures. *Mol Cell Biol* **16**, 1896-908.

Harvey, K. and Tapon, N. (2007). The Salvador-Warts-Hippo pathway - an emerging tumour-suppressor network. *Nat Rev Cancer* **7**, 182-91.

Huttlin, E. L., Ting, L., Bruckner, R. J., Gebreab, F., Gygi, M. P., Szpyt, J., Tam, S., Zarraga, G., Colby, G., Baltier, K. et al. (2015). The BioPlex Network: A Systematic Exploration of the Human Interactome. *Cell* **162**, 425-40.

Imamura, N., Horikoshi, Y., Matsuzaki, T., Toriumi, K., Kitatani, K., Ogura, G., Masuda, R., Nakamura, N., Takekoshi, S. and Iwazaki, M. (2013). Localization of aPKC lambda/iota and its interacting protein, Lgl2, is significantly associated with lung adenocarcinoma progression. *Tokai J Exp Clin Med.* **38**, 146-58.

Khadilkar, R. J., Rodrigues, D., Mote, R. D., Sinha, A. R., Kulkarni, V., Magadi, S. S. and Inamdar, M. S. (2014). ARF1-GTP regulates Asrij to provide endocytic control of *Drosophila* blood cell homeostasis. *Proc Natl Acad Sci U S A* **111**, 4898-903.

Klezovitch, O., Fernandez, T. E., Tapscott, S. J. and Vasioukhin, V. (2004). Loss of cell polarity causes severe brain dysplasia in Lgl1 knockout mice. *Genes Dev* **18**, 559-71.

Kobia, F., Duchi, S., Deflorian, G. and Vaccari, T. (2014). Pharmacologic inhibition of vacuolar H⁺ ATPase reduces physiologic and oncogenic Notch signaling. *Mol Oncol* **8**, 207-20.

Koos, B., Andersson, L., Clausson, C. M., Grannas, K., Klaesson, A., Cane, G. and Soderberg, O. (2014). Analysis of protein interactions in situ by proximity ligation assays. *Curr Top Microbiol Immunol* **377**, 111-26.

Kuphal, S., Wallner, S., Schimanski, C. C., Bataille, F., Hofer, P., Strand, S., Strand, D. and Bosserhoff, A. K. (2006). Expression of Hugel-1 is strongly reduced in malignant melanoma. *Oncogene* **25**, 103-10.

- Kux, K. and Pitsouli, C.** (2014). Tissue communication in regenerative inflammatory signaling: lessons from the fly gut. *Front Cell Infect Microbiol* **4**, 49.
- Kwon, Y., Vinayagam, A., Sun, X., Dephore, N., Gygi, S. P., Hong, P. and Perrimon, N.** (2013). The Hippo signaling pathway interactome. *Science* **342**, 737-40.
- La Marca, J. E. and Richardson, H. E.** (2020). Two-Faced: Roles of JNK Signalling During Tumourigenesis in the Drosophila Model. *Front Cell Dev Biol* **8**, 42.
- Lee, T. and Luo, L.** (2001). Mosaic analysis with a repressible cell marker (MARCM) for Drosophila neural development. *Trends Neurosci* **24**, 251-4.
- Lim, D. H., Lee, S., Han, J. Y., Choi, M. S., Hong, J. S. and Lee, Y. S.** (2019). MicroRNA miR-252 targets mbt to control the developmental growth of Drosophila. *Insect Mol Biol* **28**, 444-454.
- Lisovsky, M., Dresser, K., Baker, S., Fisher, A., Woda, B., Banner, B. and Lauwers, G. Y.** (2009). Cell polarity protein Lgl2 is lost or aberrantly localized in gastric dysplasia and adenocarcinoma: an immunohistochemical study. *Mod Pathol.* **22**, 977-84.
- Lisovsky, M., Dresser, K., Woda, B. and Mino-Kenudson, M.** (2010). Immunohistochemistry for cell polarity protein Lgl2 differentiates pancreatic intraepithelial neoplasia-3 and ductal adenocarcinoma of the pancreas from lower-grade pancreatic intraepithelial neoplasias. *Hum Pathol.* **41**, 902-9.
- Lu, X., Feng, X., Man, X., Yang, G., L., T., Du, D., F., Z., Yuan, H., Huang, Q., Zhang, Z. et al.** (2009). Aberrant splicing of Hugi-1 is associated with hepatocellular carcinoma progression. *Clin Cancer Res.* **15**, 3287-96.
- Mao, D., Lin, G., Tepe, B., Zuo, Z., Tan, K. L., Senturk, M., Zhang, S., Arenkiel, B. R., Sardiello, M. and Bellen, H. J.** (2019). VAMP associated proteins are required for autophagic and lysosomal degradation by promoting a PtdIns4P-mediated endosomal pathway. *Autophagy* **15**, 1214-1233.
- Melzer, J., Kraft, K. F., Urbach, R. and Raabe, T.** (2013). The p21-activated kinase Mbt is a component of the apical protein complex in central brain neuroblasts and controls cell proliferation. *Development* **140**, 1871-81.
- Menzel, N., Melzer, J., Waschke, J., Lenz, C., Wecklein, H., Lochnit, G., Drenckhahn, D. and Raabe, T.** (2008). The Drosophila p21-activated kinase Mbt modulates DE-cadherin-mediated cell adhesion by phosphorylation of Armadillo. *Biochem J* **416**, 231-41.

Menzel, N., Schneeberger, D. and Raabe, T. (2007). The Drosophila p21 activated kinase Mbt regulates the actin cytoskeleton and adherens junctions to control photoreceptor cell morphogenesis. *Mech Dev* **124**, 78-90.

Muthuswamy, S. K. and Xue, B. (2012). Cell polarity as a regulator of cancer cell behavior plasticity. *Annu Rev Cell Dev Biol* **28**, 599-625.

Neumuller, R. A., Wirtz-Peitz, F., Lee, S., Kwon, Y., Buckner, M., Hoskins, R. A., Venken, K. J., Bellen, H. J., Mohr, S. E. and Perrimon, N. (2012). Stringent analysis of gene function and protein-protein interactions using fluorescently tagged genes. *Genetics* **190**, 931-40.

Ntziachristos, P., Lim, J. S., Sage, J. and Aifantis, I. (2014). From fly wings to targeted cancer therapies: a centennial for notch signaling. *Cancer Cell* **25**, 318-34.

Pamarthy, S., Kulshrestha, A., Katara, G. K. and Beaman, K. D. (2018). The curious case of vacuolar ATPase: regulation of signaling pathways. *Mol Cancer* **17**, 41.

Parsons, L. M., Grzeschik, N. A. and Richardson, H. E. (2014a). Lgl Regulates the Hippo Pathway Independently of Fat/Dachs, Kibra/Expanded/Merlin and dRASSF/dSTRIPAK. *Cancers (Basel)* **6**, 879-96.

Parsons, L. M., Portela, M., Grzeschik, N. A. and Richardson, H. E. (2014b). Lgl regulates Notch signaling via endocytosis, independently of the apical aPKC-Par6-Baz polarity complex. *Curr Biol* **24**, 2073-84.

Perez-Riverol, Y., Bai, J., Bandla, C., Garcia-Seisdedos, D., Hewapathirana, S., Kamatchinathan, S., Kundu, D. J., Prakash, A., Frericks-Zipper, A., Eisenacher, M. et al. (2022). The PRIDE database resources in 2022: a hub for mass spectrometry-based proteomics evidences. *Nucleic Acids Res* **50**, D543-D552.

Petzoldt, A. G., Gleixner, E. M., Fumagalli, A., Vaccari, T. and Simons, M. (2013). Elevated expression of the V-ATPase C subunit triggers JNK-dependent cell invasion and overgrowth in a Drosophila epithelium. *Dis Model Mech* **6**, 689-700.

Pojer, J. M., Manning, S. A., Kroeger, B., Kondo, S. and Harvey, K. F. (2021). The Hippo pathway uses different machinery to control cell fate and organ size. *iScience* **24**, 102830.

Portela, M., Parsons, L. M., Grzeschik, N. A. and Richardson, H. E. (2015). Regulation of Notch signaling and endocytosis by the Lgl neoplastic tumor suppressor. *Cell Cycle* **14**, 1496-506.

- Portela, M., Yang, L., Paul, S., Li, X., Veraksa, A., Parsons, L. M. and Richardson, H. E.** (2018). Lgl reduces endosomal vesicle acidification and Notch signaling by promoting the interaction between Vap33 and the V-ATPase complex. *Sci Signal* **11**.
- Recasens-Alvarez, C., Ferreira, A. and Milan, M.** (2017). JAK/STAT controls organ size and fate specification by regulating morphogen production and signalling. *Nat Commun* **8**, 13815.
- Richardson, H. E. and Portela, M.** (2017). Tissue growth and tumorigenesis in *Drosophila*: cell polarity and the Hippo pathway. *Curr Opin Cell Biol* **48**, 1-9.
- Sanhueza, M., Chai, A., Smith, C., McCray, B. A., Simpson, T. I., Taylor, J. P. and Pennetta, G.** (2015). Network analyses reveal novel aspects of ALS pathogenesis. *PLoS Genet* **11**, e1005107.
- Schimanski, C. C., Schmitz, G., Kashyap, A., Bosserhoff, A. K., Bataille, F., Schafer, S. C., Lehr, H. A., Berger, M. R., Galle, P. R., Strand, S. et al.** (2005). Reduced expression of Hugel-1, the human homologue of *Drosophila* tumour suppressor gene lgl, contributes to progression of colorectal cancer. *Oncogene* **24**, 3100-9.
- Schneeberger, D. and Raabe, T.** (2003). Mbt, a *Drosophila* PAK protein, combines with Cdc42 to regulate photoreceptor cell morphogenesis. *Development* **130**, 427-37.
- Schroeder, M. C., Chen, C. L., Gajewski, K. and Halder, G.** (2013). A non-cell-autonomous tumor suppressor role for Stat in eliminating oncogenic scribble cells. *Oncogene* **32**, 4471-9.
- Soderberg, O., Gullberg, M., Jarvius, M., Ridderstrale, K., Leuchowius, K. J., Jarvius, J., Wester, K., Hydbring, P., Bahram, F., Larsson, L. G. et al.** (2006). Direct observation of individual endogenous protein complexes in situ by proximity ligation. *Nat Methods* **3**, 995-1000.
- Stephens, R., Lim, K., Portela, M., Kvensakul, M., Humbert, P. O. and Richardson, H. E.** (2018). The Scribble Cell Polarity Module in the Regulation of Cell Signaling in Tissue Development and Tumorigenesis. *J Mol Biol*.
- Sun, S., Reddy, B. V. and Irvine, K. D.** (2015). Localization of Hippo signalling complexes and Warts activation in vivo. *Nat Commun* **6**, 8402.
- Tsuda, H., Han, S. M., Yang, Y., Tong, C., Lin, Y. Q., Mohan, K., Haueter, C., Zoghbi, A., Harati, Y., Kwan, J. et al.** (2008). The amyotrophic lateral sclerosis 8 protein VAPB is cleaved, secreted, and acts as a ligand for Eph receptors. *Cell* **133**, 963-77.

Vaccari, T., Duchi, S., Cortese, K., Tacchetti, C. and Bilder, D. (2010). The vacuolar ATPase is required for physiological as well as pathological activation of the Notch receptor. *Development* **137**, 1825-32.

Venken, K. J., Schulze, K. L., Haelterman, N. A., Pan, H., He, Y., Evans-Holm, M., Carlson, J. W., Levis, R. W., Spradling, A. C., Hoskins, R. A. et al. (2011). MiMIC: a highly versatile transposon insertion resource for engineering *Drosophila melanogaster* genes. *Nat Methods* **8**, 737-43.

Vergheze, S. and Moberg, K. (2019). Roles of Membrane and Vesicular Traffic in Regulation of the Hippo Pathway. *Front Cell Dev Biol* **7**, 384.

Vlachos, S. and Harden, N. (2011). Genetic evidence for antagonism between Pak protein kinase and Rho1 small GTPase signaling in regulation of the actin cytoskeleton during *Drosophila* oogenesis. *Genetics* **187**, 501-12.

Wang, Y., Zhang, H., Shi, M., Liou, Y. C., Lu, L. and Yu, F. (2017). Sec71 functions as a GEF for the small GTPase Arf1 to govern dendrite pruning of *Drosophila* sensory neurons. *Development* **144**, 1851-1862.

Zhou, W., Li, X. and Premont, R. T. (2016). Expanding functions of GIT Arf GTPase-activating proteins, PIX Rho guanine nucleotide exchange factors and GIT-PIX complexes. *J Cell Sci* **129**, 1963-74.

Figures

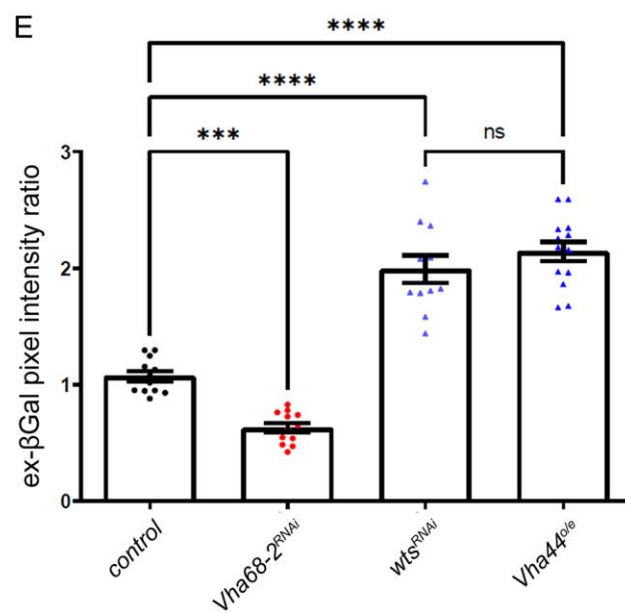
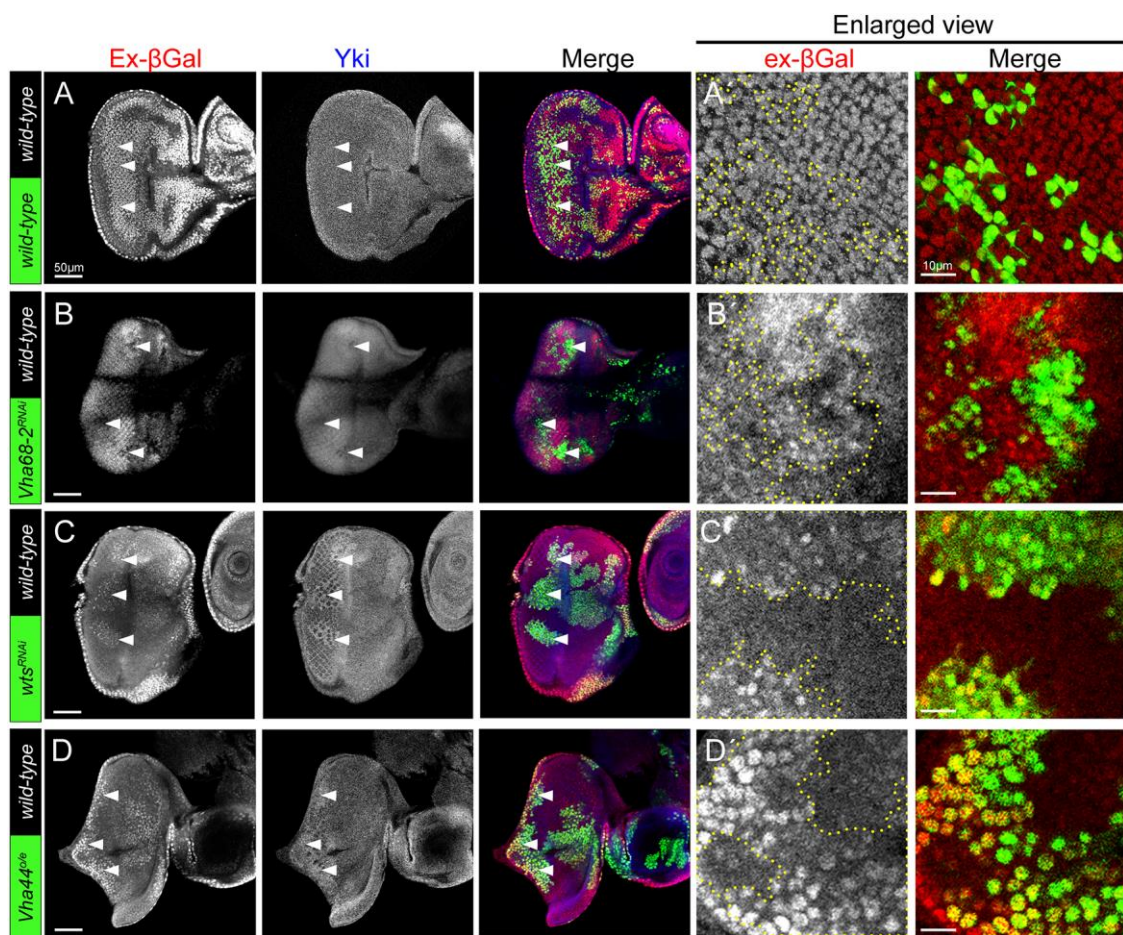


Fig 1. The Hippo signalling pathway is negatively regulated by V-ATPase activity in *Drosophila*.

(A-D) Confocal planar sections of mosaic eye discs containing the Yki target reporter, *ex-lacZ*, stained for β Gal (grey, or red in merges), and for Yki (grey, or blue in merges). Example GFP-positive clones are indicated by arrowheads. (A) Example of a control mosaic disc showing endogenous expression of *ex-lacZ* and Yki in the eye epithelium. (B) Example of a *Vha68-2^{RNAi}* mosaic disc, with RNAi-expressing clones being GFP-positive. *Vha68-2* knockdown leads to downregulation of the Yki target, *ex-lacZ* (β Gal) reporter and Yki levels. (C) Example of a *wt^{sRNAi}* mosaic disc with RNAi-expressing clones being GFP-positive. *wt^s* knockdown leads to upregulation of the Yki target, *ex-lacZ* (β Gal) reporter and Yki levels. (D) Example of a *Vha44* overexpression mosaic disc, with *Vha44* overexpressing clones being GFP-positive. *Vha44* overexpression leads to upregulation of the Yki target, *ex-lacZ* (β Gal) reporter and Yki levels. (A', B', C', D') Higher magnification examples of *ex-lacZ* (β Gal) stainings in GFP-positive clones for the different samples. (E) Quantification of the *ex-lacZ* (β Gal) pixel intensity ratio of the transgenic clones compared to *wild-type* clones. Error bars represent SEM. **** P-value<0.0001 *** P-value=0.0009 (one-way ANOVA with Bonferroni post-test). The scale bar represents 50 μ m and in A'-D' the scale bar represents 10 μ m. Posterior is to the left in all images.

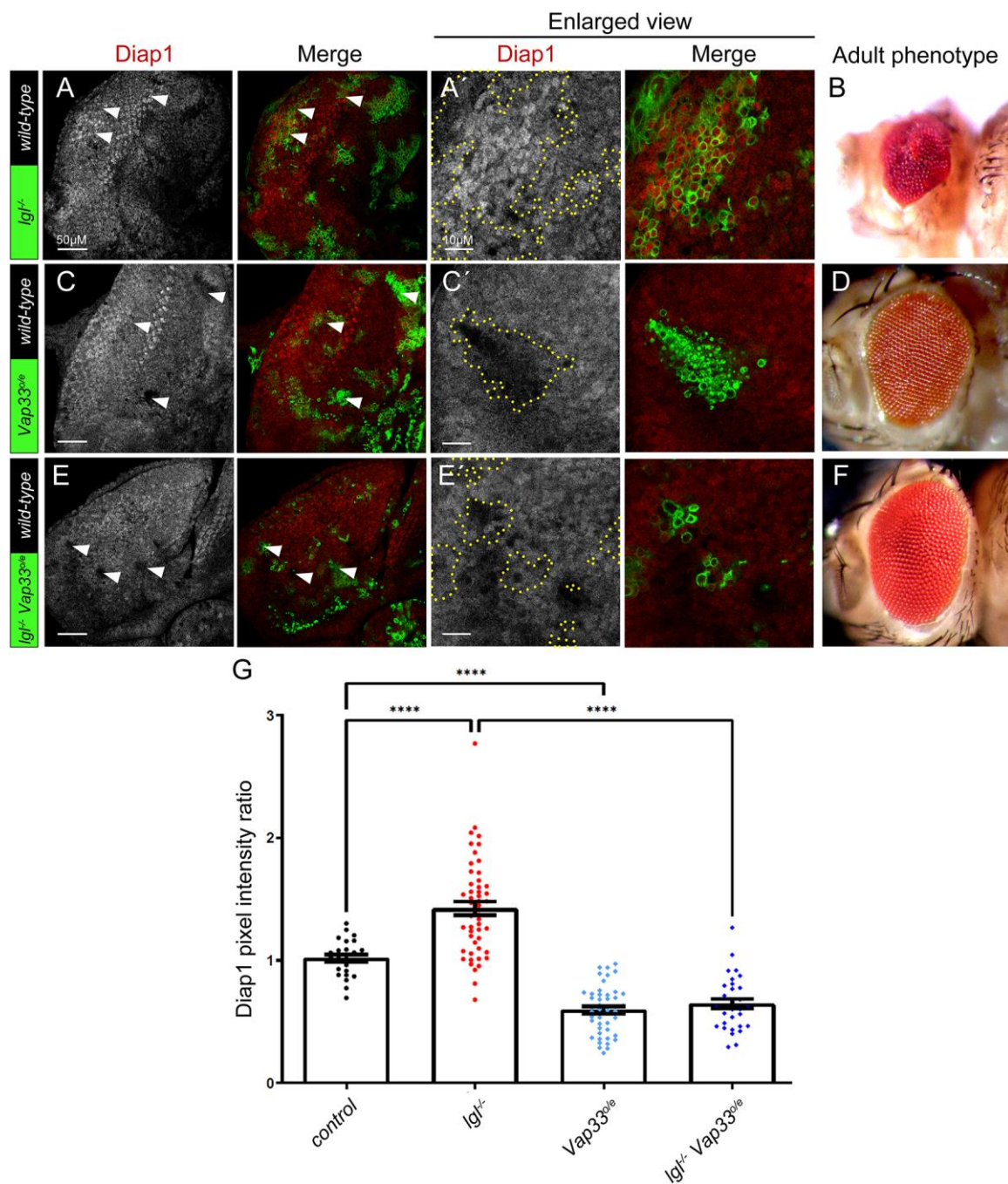


Fig. 2. Vap33 activates the Hippo pathway.

(A, C, E) Confocal planar sections of mosaic eye discs, stained for the Yki target Diap1 (grey, or red in merges). Mutant clones are GFP-positive, and examples are indicated by arrowheads. (A) Example of a *lgl*^{-/-} mosaic disc showing elevated Diap1 levels in the mutant clones. (B) *lgl*^{-/-} mosaic adult female eye, showing a distorted disorganized eye phenotype. (C) Example of *Vap33*^{o/e} mosaic disc showing reduced Diap1 levels. (D) *Vap33*^{o/e} mosaic adult

female eye, showing slight disorganization in the arrangement of ommatidia. (E) Example of *Igf Vap33^{0/e}* mosaic disc showing normalized Diap1 levels. (F) *Igf Vap33^{0/e}* mosaic adult female eye, showing only slight disorganization of the ommatidial arrangement. (A', C', E') higher magnifications of Diap1 stainings for the different mosaic tissues. (G) Quantification of Diap1 pixel intensity ratio of mutant/transgenic clones compared with *wild-type* clones. Error bars represent SEM. **** P-value<0.0001 (one-way ANOVA with Bonferroni post-test). In A, C, E, the scale bar represents 50 μ m, and in A', C', E' the scale bar represents 10 μ m. Posterior is to the left in all images.

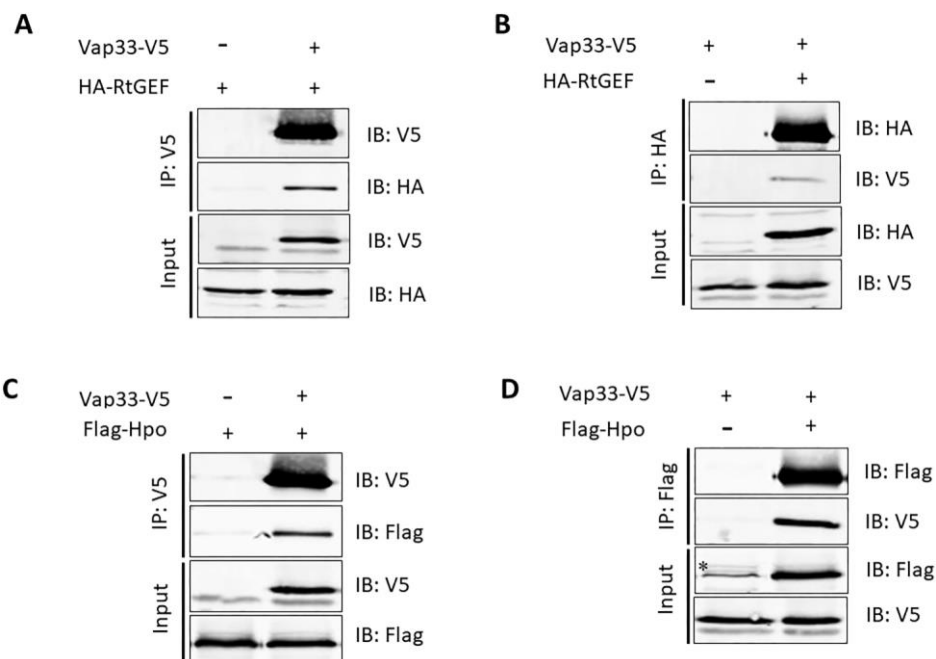


Fig 3. Vap33 interacts with RtGEF and Hpo in S2 cells.

(A-D) Indicated protein constructs were expressed in S2 cells, and protein interactions were analysed by co-immunoprecipitation (co-IP). IP: immunoprecipitation antibody; IB: immunoblot antibody. Asterisk in (D) indicates non-specific band.

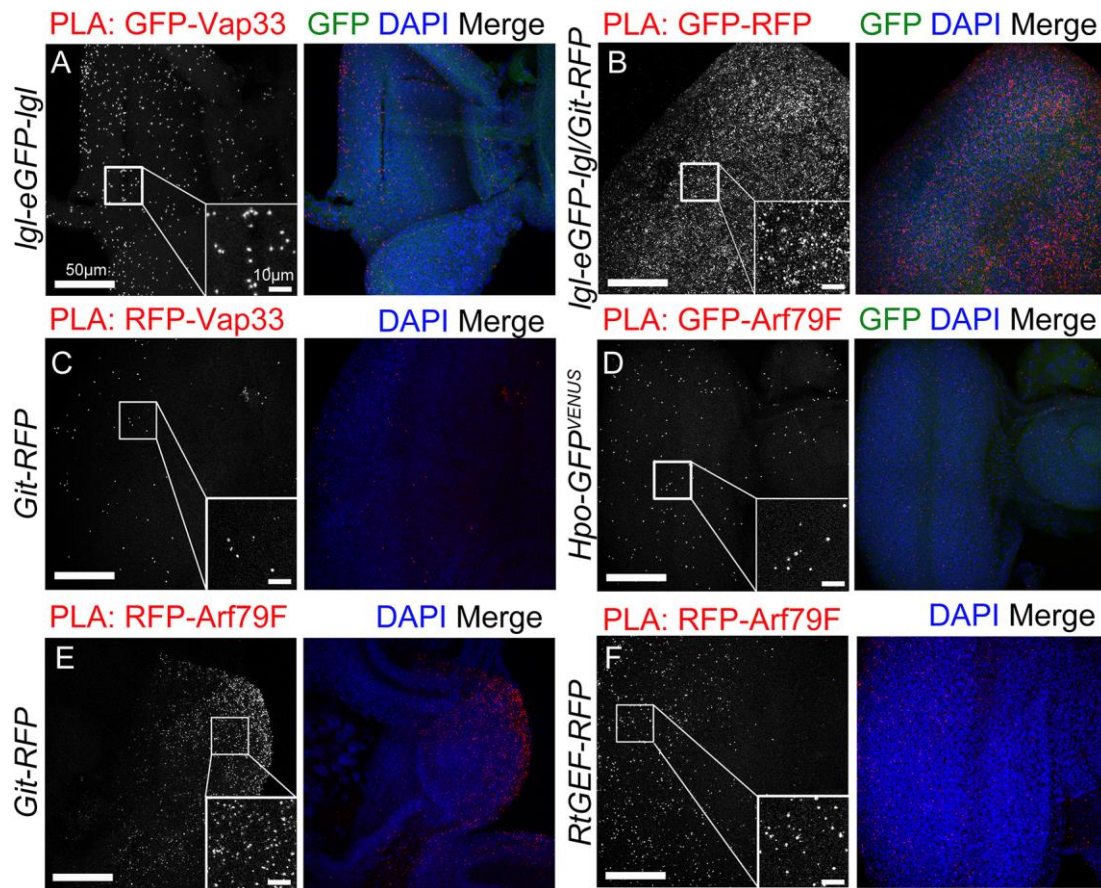


Fig. 4. Vap33 interacts with Git, Arf79F interacts with Git, RtGEF and Hpo, and Lgl interacts with Vap33 and Git *in vivo*.

(A-F) Confocal planar images showing *in situ* proximity ligation assays (PLAs) in third instar larval eye discs. Positive PLA results between the indicated proteins are visualized by punctate signal (grey or red in the merges). Nuclei are stained with DAPI (blue). Insets show high magnification images of the PLA foci. (A) Positive-control PLA in *lgl-eGFP-lgl* eye discs using antibodies against GFP and Vap33. (B) PLA in *lgl-eGFP-lgl/Git-RFP* eye discs using antibodies against RFP and GFP. (C) PLA in *Git-RFP* eye discs using antibodies against RFP and Vap33. (D) PLA in *Hpo-GFP* eye discs using antibodies against GFP and Arf79F. (E) PLA in *Git-RFP* eye discs using antibodies against RFP and Arf79F. (F) PLA in *RtGEF-RFP* eye discs using antibodies against RFP and Arf79F. Scale bars represent 50 μm.

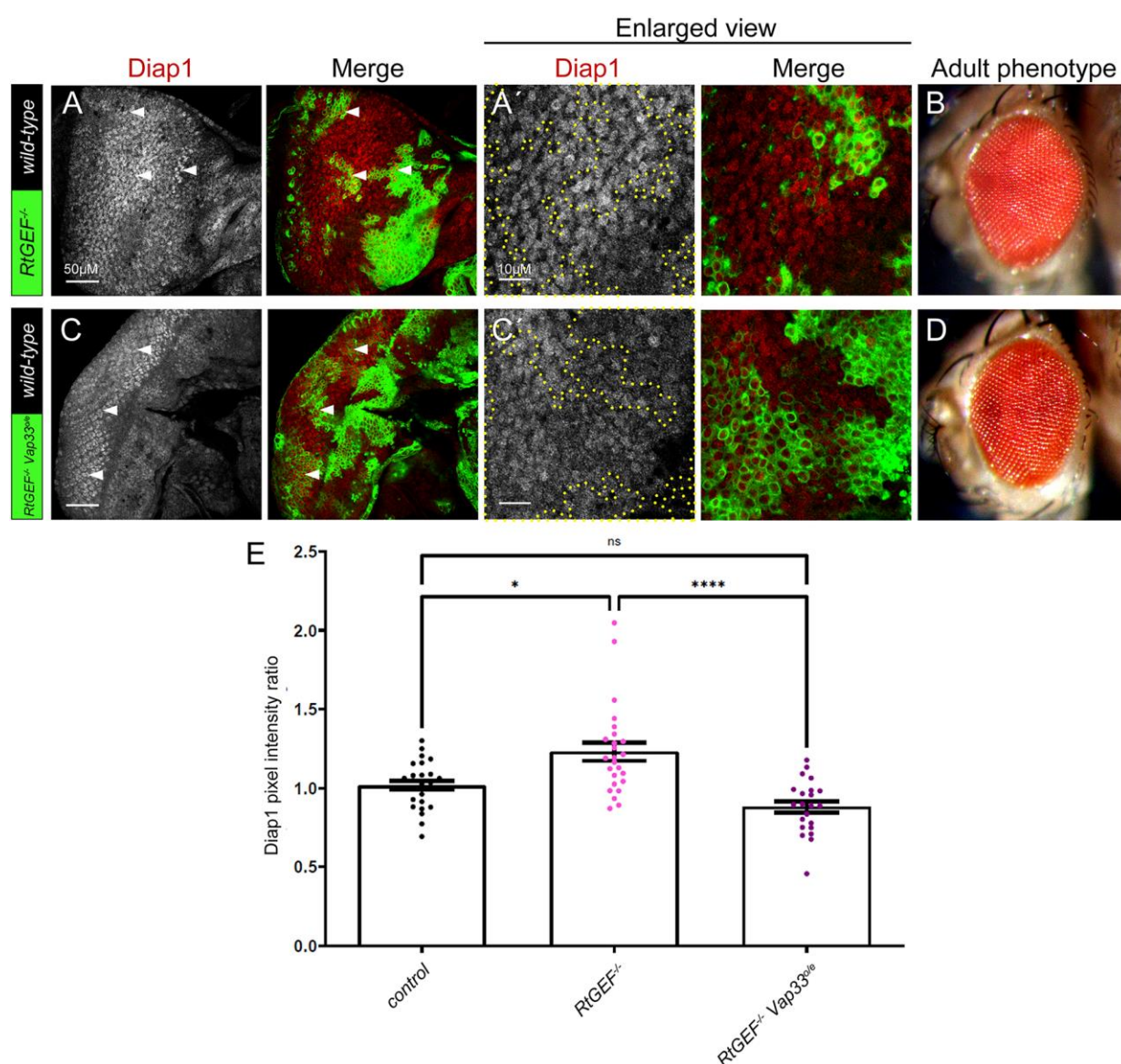


Fig. 5. Vap33 overexpression rescues increased Hippo pathway target gene expression in *RtGEF* mutant tissue.

(A) Confocal planar section of a *RtGEF* mosaic disc stained for the Yki target Diap1 (grey, or red in merges, mutant clones are GFP-positive, examples indicated by arrowheads). (B) *RtGEF* mosaic adult female eye showing a mostly *wild-type* appearance. (C) Confocal planar section of *RtGEF Vap33^{oe}* mosaic disc stained for Diap1 (grey, or red in merge, mutant tissue is GFP-positive, examples indicated by arrowheads). (D) *RtGEF Vap33^{oe}* mosaic adult female eye showing slight disorganization of the ommatidial arrangement, similar to *Vap33^{oe}* mosaic eyes (Fig 2D). (A', C') higher magnifications of Diap1 stainings of the

respective samples. (E) Quantification of Diap1 pixel intensity ratio of mutant/transgenic clones compared to *wild-type* clones. Error bars represent SEM. **** P-value<0.0001 * P-value=0.019 n.s., differences not significant (one-way ANOVA with Bonferroni post-test). Posterior is to the left. Scale bar represents 50 μm (A, C) and 10 μm (A' C').

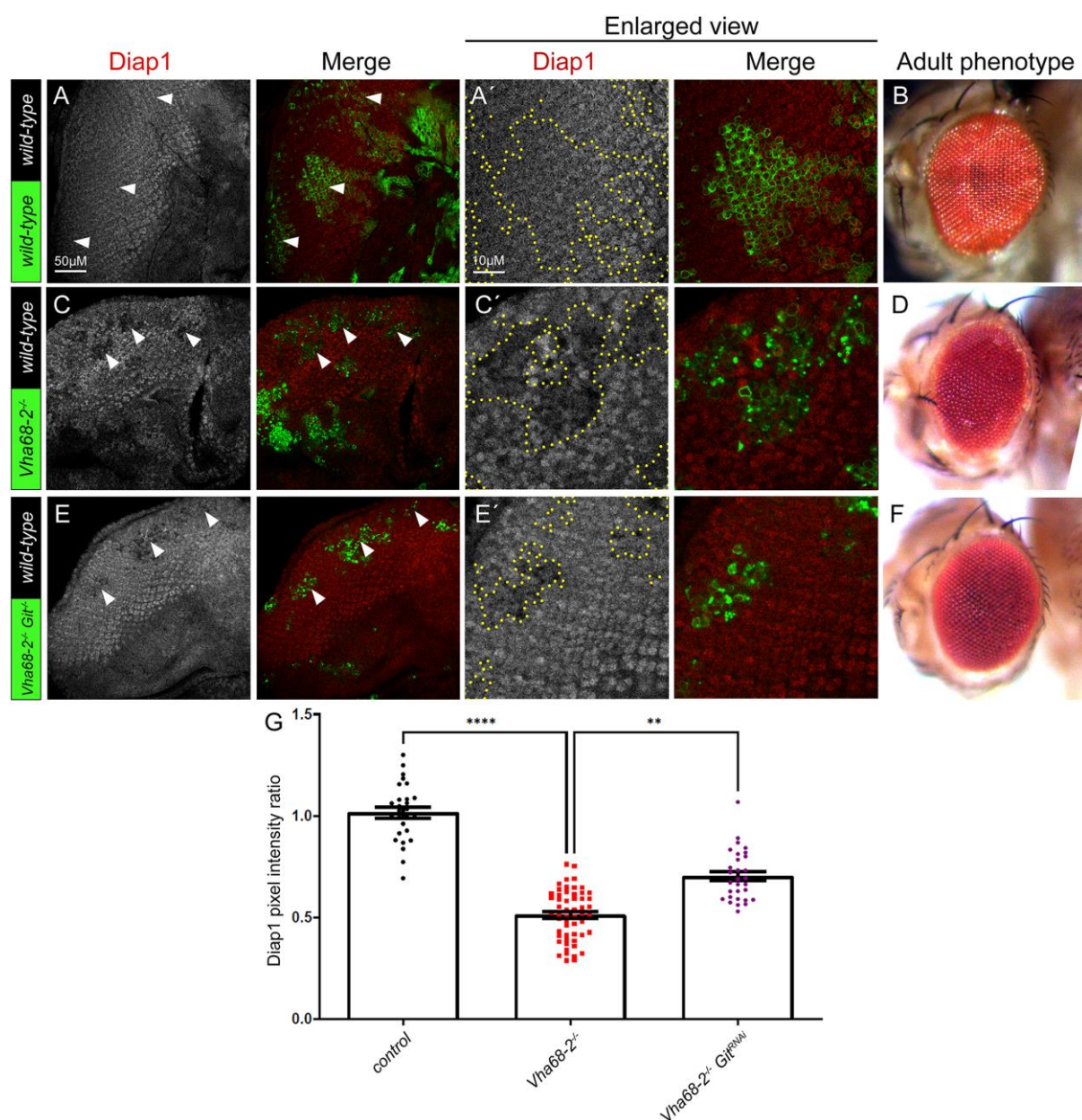


Fig. 6. *Git* knockdown rescues the reduced Hippo pathway target gene expression in *Vha68-2* mutant clones.

(A) Confocal planar section of control mosaic eye discs (clones marked with GFP) stained for the Yki target Diap1 (grey, or red in merges, example GFP-positive clones indicated by arrowheads) showing endogenous expression of Diap1. (B) Control mosaic adult female eye. (C) Confocal planar section of *Vha68-2*⁺ mosaic disc stained for Diap1 (grey, or red in merges, mutant clones are GFP-positive, examples indicated by arrowheads). (D) *Vha68-2*⁺ mosaic adult female eye showing disorganization of the ommatidial arrangement. (E)

Confocal planar section of *Vha68-2^{-/-} Git^{RNAi}* mosaic disc stained for Diap1 (grey, or red in merge, mutant tissue is GFP-positive, examples indicated by arrowheads). (F) *Vha68-2^{-/-} Git^{RNAi}* mosaic adult female eye showing a mostly normal phenotype. (A', C', E') Higher magnifications of Diap1 stainings of the corresponding samples. (G) Quantification of Diap1 pixel intensity ratio of the mutant/transgenic clones relative to *wild-type* clones. Error bars represent SEM. **** P-value<0.0001 ** P-value=0.054 (one-way ANOVA with Bonferroni post-test). In all images, posterior is to the left. Scale bar represent 50 μm (A, C, E), and 10 μm (A', C', E').

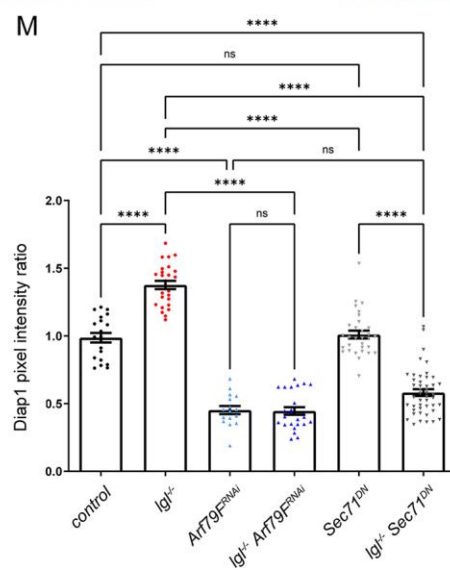
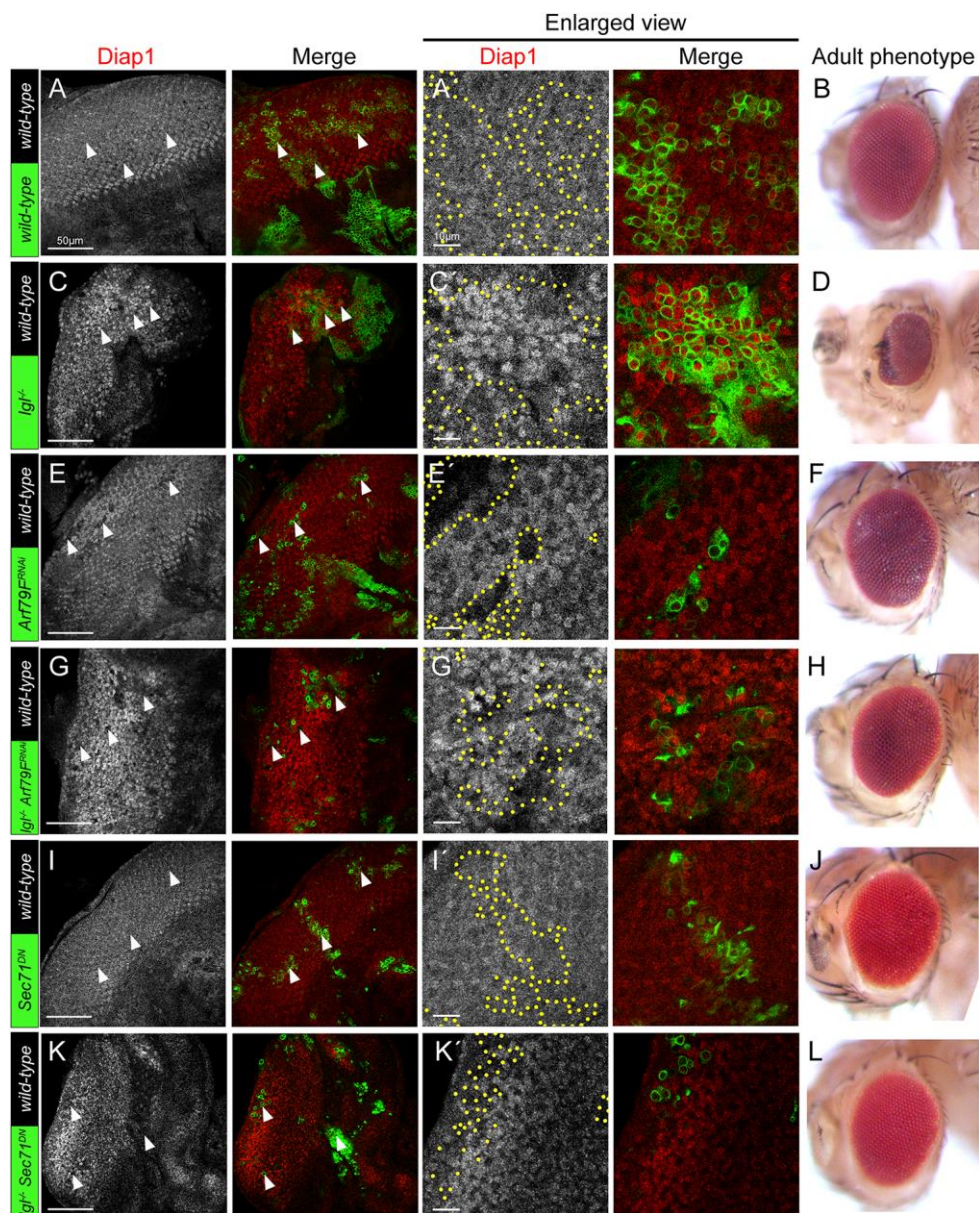


Fig. 7. Knockdown of Arf79F prevents the upregulation of Hippo pathway targets.

(A, C, E, G, I, K) Confocal planar images of mosaic third instar larval eye-antennal discs, stained for the Yki target, Diap1 (grey, or red in merge). In all instances, example GFP-positive clones are marked by arrowheads. (A) Control eye discs (clones marked by GFP) showing endogenous expression of Diap1. (B) Control mosaic adult female eye. (C) *lgl* mosaic disc showing elevated Diap1 expression in mutant clones (GFP-positive). (D) *lgl* mosaic adult female eye showing a distorted eye with disorganized arrangements of ommatidia. (E) *Arf79F^{RNAi}* mosaic disc showing reduced Diap1 expression in transgene-expressing clones (GFP-positive). (F) *Arf79F^{RNAi}* mosaic adult female eye showing slightly disorganized ommatidia arrangements. (G) *lgl Arf79F^{RNAi}* mosaic disc showing reduced Diap1 expression in mutant/transgene-expressing clones (GFP-positive). (H) *lgl Arf79F^{RNAi}* mosaic adult female eye showing a mostly normal eye with only some slightly disorganized ommatidia arrangements. (I) *Sec71^{DN}* mosaic disc showing normal Diap1 expression in transgene-expressing clones (GFP-positive). (J) *Sec71^{DN}* mosaic adult female eye showing slightly disorganized ommatidia arrangements. (K) *lgl Sec71^{DN}* mosaic disc showing reduced Diap1 expression in mutant/transgene-expressing clones (GFP-positive). (L) *lgl Sec71^{DN}* mosaic adult female eye showing a mostly normal eye with only some slightly disorganized ommatidia arrangements. (A', C', E', G', I', K') higher magnifications of Diap1 stainings in the corresponding samples. (M) Quantification of Diap1 pixel intensity ratio of mutant/transgene clones relative to *wild-type* clones. Error bars represent SEM. **** P-value<0.0001 (one-way ANOVA with Bonferroni post-test). Posterior is to the left in all images. Scale bars represents 50 μ m (A, C, E, G, I, K), or 10 μ m (A', C', E', G', I', K').

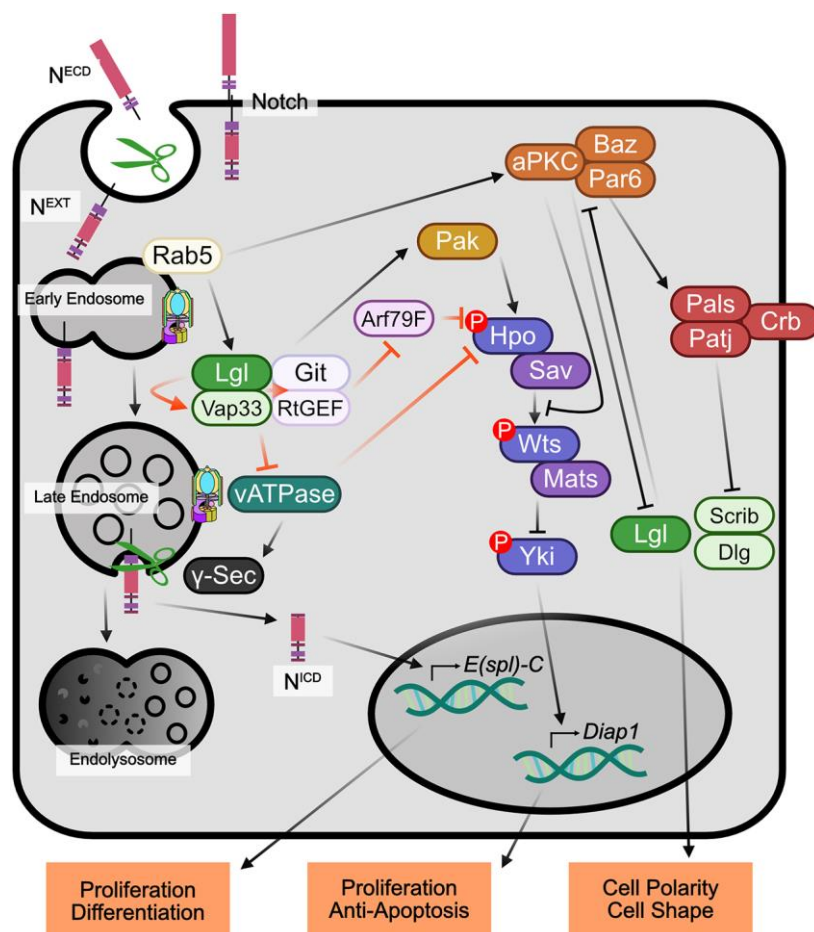


Fig. 8. Model for the regulation of Hippo and Notch signalling by Lgl/aPKC.

Lgl/Vap33 have a dual action in activating Hippo signalling: 1) through binding to RtGEF/Git, which opposes Arf79F inhibition of Hpo, and 2) by binding to V-ATPase components and inhibiting V-ATPase activity, which is an inhibitor of Hippo signalling. The Lgl interactor, Rab5, may be involved to link Lgl and Vap33 to early endosomes. It is possible that the RtGEF/Git interacting protein kinase, Pak (Pak1, Pak3, Mbt), is involved in activating Hpo downstream of Git/RtGEF. By reducing V-ATPase activity, Lgl/Vap33 inhibits Notch signalling by decreasing the production of the active N^{ICD} isoform by γ -Secretase in endosomes, thereby leading to lower expression of Notch targets, such as *E(Spl)-C* genes. Lgl also opposes aPKC activity, and in mammalian cells elevated PKC inhibits Hippo signalling by sequestering Hpo (MST1/2) away from its target, Wts (LATS). Orange arrows indicate the parts of this model that we have provided evidence for in this study.

Supplementary Figure 1

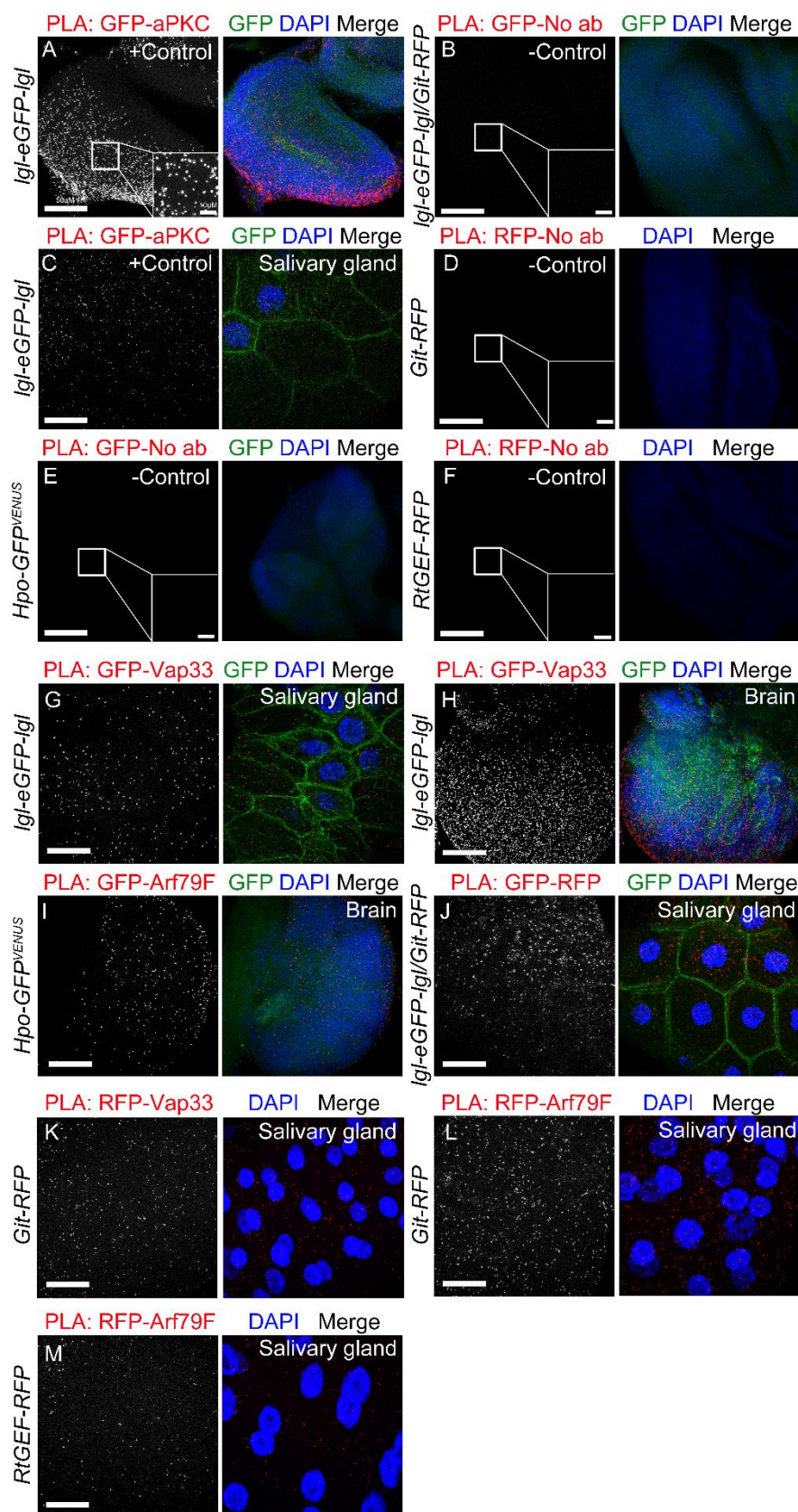


Fig. S1. RtGEF interacts with Arf79F, Vap33, Lgl and Arf79F interact with Git in the salivary glands, and Arf79F in the brain.

(A-M) Confocal planar images showing *in situ* proximity ligation assay (PLA) on third instar larval eye discs, brains or salivary glands. Positive PLA results appear as punctate signals (grey, or red in the merges). Nuclei are stained with DAPI (blue). Insets show high magnification images of the PLA foci. (A) Positive-control PLA on *lgl-eGFP-lgl* eye discs using antibodies against GFP and aPKC. (B) Negative control PLA in *lgl-eGFP-lgl/Git-RFP* eye discs using only one primary antibody against GFP. (C) Positive-control PLA in *lgl-eGFP-lgl* salivary glands using antibodies against GFP and aPKC. (D) Negative control PLA on *Git-RFP* eye discs using only one primary antibody against RFP. (E) Negative control PLA in *Hpo-GFP* eye discs using only one primary antibody against GFP. (F) Negative control PLA in *RtGEF-RFP* eye discs using only one primary antibody against RFP. (G, H) Positive-control PLA on *lgl-eGFP-lgl* salivary glands (G) and brains (H) using antibodies against GFP and Vap33. (I) PLA in *Hpo-GFP* brains using antibodies against GFP and Arf79F. (J) PLA in *lgl-eGFP-lgl/Git-RFP* salivary glands using antibodies against RFP and GFP. (K) PLA in *Git-RFP* salivary glands using antibodies against RFP and Vap33. (L) PLA in *Git-RFP* salivary glands using antibodies against RFP and Arf79F. (M) PLA in *RtGEF-RFP* salivary glands using antibodies against RFP and Arf79F. Scale bars represent 50 μ m.

Supplementary Figure 2

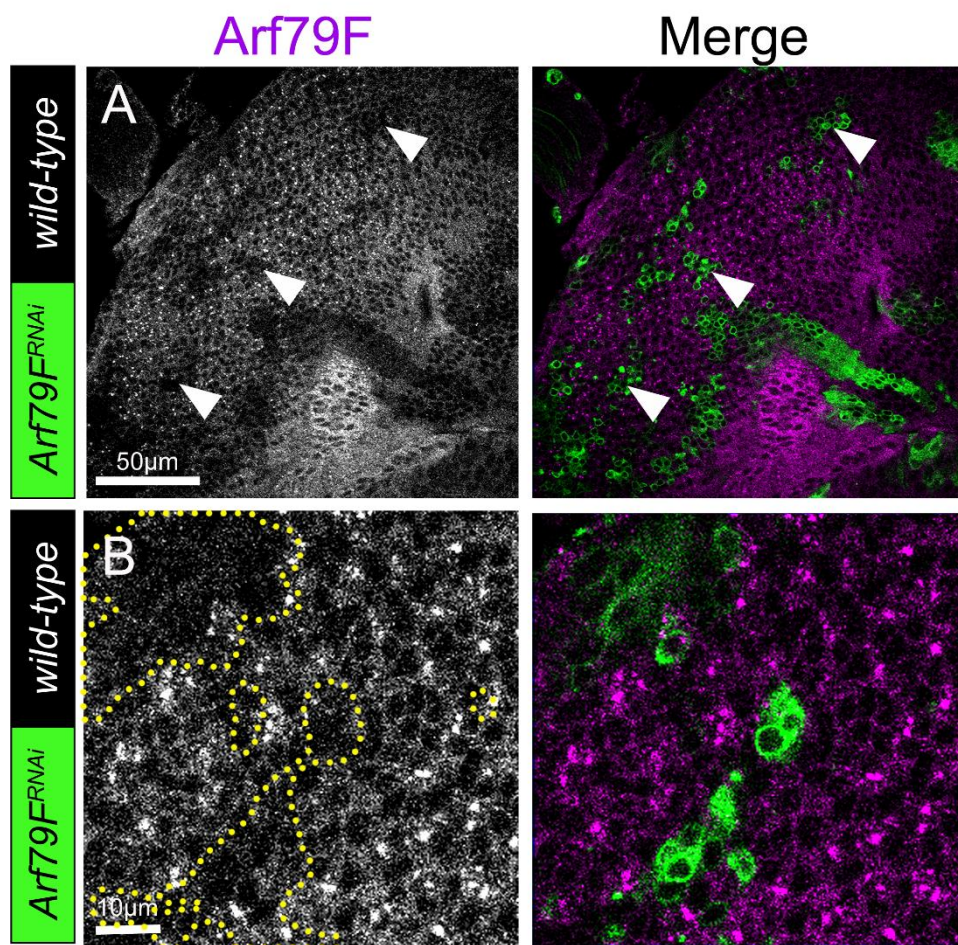


Fig. S2. Arf79F staining in *Arf79F* knockdown mosaic eye-antennal discs.

(A) Confocal planar sections of *Arf79F*^{RNAi} mosaic third instar larval eye-antennal discs (clones marked by GFP) stained for Arf79F (magenta). Knockdown of Arf79F using the *Arf79F*^{RNAi} line reduced the amount of Arf79F protein in the *Arf79F*^{RNAi} GFP-positive clones (green, example clones marked by arrowheads). Higher magnification shown in (B). Scale bars represent 50 μm (A) or 10 μm (B).

Supplementary Figure 3

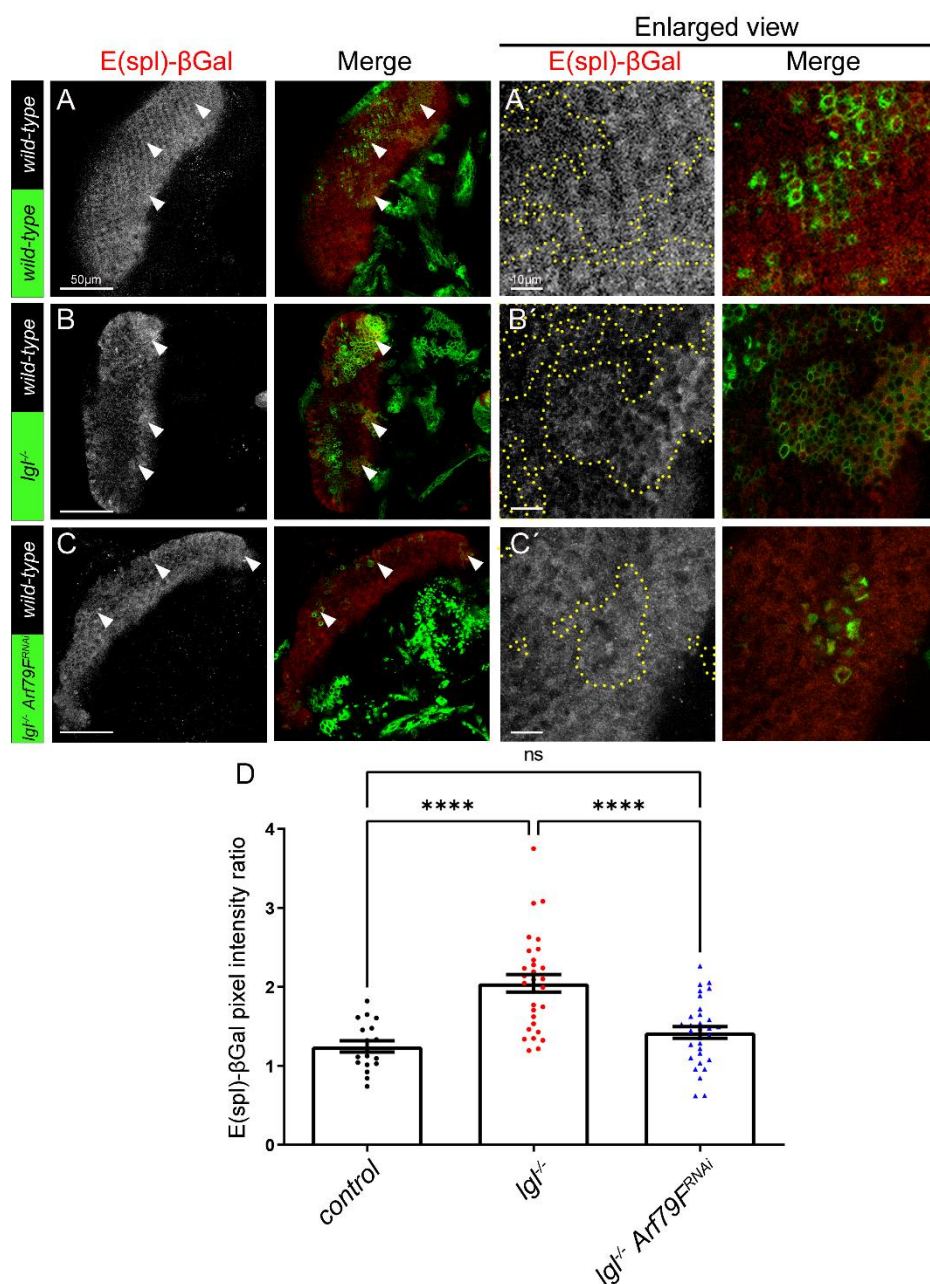


Fig. S3. Knockdown of *Arf79F* prevents Notch signalling pathway upregulation in *lgl* mutant tissue.

(A-C) Confocal planar sections of a mosaic eye discs containing the Notch target *E(spl)lacZ* reporter, stained for β Gal (grey, or red in merges, example clones marked by arrowheads). (A) Control mosaic disc showing endogenous expression of *E(spl)lacZ*

within and posterior to the morphogenetic furrow (arrowheads indicate clones showing normal *E(spl)lacZ* expression). (B) *lgl* mosaic disc (mutant clones are GFP-positive). (C) *lgl Arf79F^{RNAi}* (mutant clones are GFP-positive). (D) Quantification of β Gal pixel intensity ratio between *wild-type* clones compared to mutant/transgenic clones. Error bars represent SEM. **** P-value<0.0001 (one-way ANOVA with Bonferroni post-test). In all images, posterior is to the left, and the scale bars represent 50 μ m. (A', B', C') Higher magnifications of β Gal stainings (grey, or red in merges, mutant clones are GFP-positive) for all genotypes. Scale bars represent 10 μ m.

Table S1. *Drosophila* stocks

<u>Drosophila stock</u>	<u>Source and reference</u>
<i>l(2)gl^{27S3}</i> (denoted as <i>lgl^{27S3}</i>)	(Grzeschik et al., 2007)
<i>P(E(spl)m8-HLH-2.61)2</i> (denoted as <i>E(spl)lacZ^{m8-2.61}</i> or <i>E(spl)lacZ</i> .)	A. Bergmann (Kramatschek and Campos-Ortega, 1994) on chromosome 2R (Christiansen et al., 2013)
<i>P(UAS-lacZ.nls)</i> (denoted as <i>UAS-lacZ-nls (III)</i>)	G. Baeg
<i>P(UAS-Vha44.P)</i> (denoted as <i>UAS-Vha44</i>)	M. Simons (Petzoldt et al., 2013)
<i>Vha68-2^{R6}</i> (EMS generated null mutant, due to stop codon mutation)	BL39621, Bloomington Stock Center (Vaccari et al., 2010)
<i>P(y[+t7.7] w[+mC]=10XUAS-mCD8::GFP)attP2</i> (denoted as <i>UAS-CD8-GFP</i> .)	BL32184, Bloomington Stock Center
<i>Mi(y[+mDint2]=MIC)l(2)gl[MI07575]</i> (denoted as <i>MI07575 lgl-eGFP-lgl</i>)	BL43734, Bloomington Stock Center (Venken et al., 2011)
<i>P(w[+mC]=UAS-Vap-33-1.P)3</i> (denoted as <i>UAS-Vap33</i>)	BL26693, Bloomington Stock Center (Pennetta et al., 2002)
<i>P(TRiP.JF01355)attP2</i> (denoted as <i>UAS-luciferase^{RNAi}</i>)	BL31603, Bloomington Stock Center
<i>P(ey3.5-FLP.B)1, y¹ w[*]; P(w[+mC]=UAS-mCD8::GFP.L)Ptp4E(LL4); P(w[+mC]=tubP-GAL80)LL10 P(ry[+t7.2]=neoFRT)40A; P(w[+mC]=tubP-GAL4)LL7</i> (denoted as <i>ey-FLP, UAS-GFP; Tub-GAL80, FRT40A; Tub-GAL4/TM6B (ey-FLP MARCM 2L)</i>).	(Grzeschik et al., 2010)
<i>y[1] w[*]; Pvr[1] P(ry[+t7.2]=neoFRT)40A</i> (denoted as <i>FRT40A</i>).	BL58427, Bloomington Stock Center
<i>w; Vha68-2 RNAi TRiP.HMS01056}attP2</i>	BL34582, Bloomington Stock Center
<i>w;; UAS-Arf79F^{RNAi}</i>	VDRC 23082 and BL66175
<i>w; UAS-Sec7I^{DN}</i>	Fengwei Yu (Wang et al., 2017)

<i>w; Git-tRFP</i>	(Dent et al., 2019)
<i>w; Hpo-VENUS</i>	(Pojer et al., 2021)
<i>w; RtGEF-tRFP</i>	(Dent et al., 2019)
<i>w; FRT40A, RtGEF^{I036}/CyO-GFP</i>	(Dent et al., 2019)
<i>y v;; UAS-Git^{RNAi}</i>	BL31583
<i>w;; UAS-wts^{RNAi}</i>	NIG 12072R-1
<i>ex-lacZ</i>	BL44248
<i>yw hs-FLP;; Act>CD2>GAL4, UAS-GFP</i>	R. Mann

Table S2. List of genotypes of the samples used in each Figure.

Figure 1	Genotype
(A)	<i>yw hs-FLP; ex-lacZ/ CyO; Act>CD2>GAL4, UAS-GFP/UAS-luciferase^{RNAi}</i>
(B)	<i>yw hs-FLP; ex-lacZ/ CyO; Act>CD2>GAL4, UAS-GFP/UAS-Vha86-2^{RNAi}</i>
(C)	<i>yw hs-FLP; ex-lacZ/ CyO; Act>CD2>GAL4, UAS-GFP/UAS-wts^{RNAi}</i>
(D)	<i>yw hs-FLP; ex-lacZ/ CyO; Act>CD2>GAL4, UAS-GFP/UAS-Vha44</i>
Figure 2	
(A-B)	<i>w, eyFLP, UAS-GFP; lgl27S3, FRT40A; Tub-GAL80, FRT40A, Tub-GAL4</i>
(C-D)	<i>w, eyFLP, UAS-GFP; FRT40A; UAS-Vap33o/e /Tub-GAL80, FRT40A, Tub-GAL4</i>
(E-F)	<i>w, eyFLP, UAS-GFP; lgl27S3, FRT40A; UAS-Vap33o/e /Tub-GAL80, FRT40A, Tub-GAL4</i>
Figure 4	
(A)	<i>y,w; MiMIC lgl-eGFP-lgl MI07575</i>
(B)	<i>w; y,w; MiMIC lgl-eGFP-lgl MI07575/Git-RFP</i>
(C, E)	<i>w; Git-RFP</i>
(D)	<i>w; Hpo-GFP</i>
(F)	<i>w; RtGEF-RFP</i>
Figure S1	Related to Figure 4
(A, C, G, H)	<i>y,w; MiMIC lgl-eGFP-lgl MI07575</i>
(B, J)	<i>y,w; MiMIC lgl-eGFP-lgl MI07575/Git-RFP</i>
(D, K, L)	<i>w; Git-RFP</i>
(E, I)	<i>w; Hpo-GFP</i>
(F, M)	<i>w; RtGEF-RFP</i>
Figure 5	
(A-B)	<i>w, eyFLP, UAS-GFP; FRT40A; UAS-Vap33o/e /Tub-GAL80, FRT40A, Tub-GAL4</i>

(C-D)	<i>w, eyFLP, UAS-GFP; RtGEF, FRT40A; UAS-Vap33o/e /Tub-GAL80, FRT40A, Tub-GAL4</i>
Figure 6	
(A-B)	<i>w, eyFLP, UAS-GFP; FRT40A; Tub-GAL80, FRT40A, Tub-GAL4</i>
(C-D)	<i>w, eyFLP, UAS-GFP; Vha68-2, FRT40A; Tub-GAL80, FRT40A, Tub-GAL4</i>
(E-F)	<i>w, eyFLP, UAS-GFP; Vha68-2, FRT40A; UAS-Git^{RNAi} /Tub-GAL80, FRT40A, Tub-GAL4</i>
Figure 7	
(A-B)	<i>w, eyFLP, UAS-GFP; FRT40A; Tub-GAL80, FRT40A, Tub-GAL4</i>
(C-D)	<i>w, eyFLP, UAS-GFP; lgl27S3, FRT40A; Tub-GAL80, FRT40A, Tub-GAL4</i>
(E-F)	<i>w, eyFLP, UAS-GFP; FRT40A; UAS-Arf79F^{RNAi} /Tub-GAL80, FRT40A, Tub-GAL4</i>
(G-H)	<i>w, eyFLP, UAS-GFP; lgl27S3, FRT40A; UAS-Arf79F^{RNAi} /Tub-GAL80, FRT40A, Tub-GAL4</i>
(I-J)	<i>w, eyFLP, UAS-GFP; FRT40A, UAS-Sec71^{DN}; Tub-GAL80, FRT40A, Tub-GAL4</i>
(K-L)	<i>w, eyFLP, UAS-GFP; lgl27S3, FRT40A, UAS-Sec71^{DN}; Tub-GAL80, FRT40A, Tub-GAL4</i>
Figure S2	Related to Figure 7
(A-B)	<i>w, eyFLP, UAS-GFP; FRT40A; UAS-Arf79F^{RNAi} /Tub-GAL80, FRT40A, Tub-GAL4</i>
Figure S3	Related to Figure 7
(A)	<i>w, eyFLP, UAS-GFP; FRT40A, E(spl)m8-lacZ; Tub-GAL80, FRT40A, Tub-GAL4</i>
(B)	<i>w, eyFLP, UAS-GFP; lgl27S3, FRT40A, E(spl)m8-lacZ; Tub-GAL80, FRT40A, Tub-GAL4</i>
(C)	<i>w, eyFLP, UAS-GFP; lgl27S3, FRT40A, E(spl)m8-lacZ; UAS-Arf79F^{RNAi} /Tub-GAL80, FRT40A, Tub-GAL4</i>

Table S3.

Available for download at

<https://journals.biologists.com/jcs/article-lookup/doi/10.1242/jcs.261917#supplementary-data>

Supplementary References

- Christiansen, A. E., Ding, T., Fan, Y., Graves, H. K., Herz, H. M., Lindblad, J. L. and Bergmann, A.** (2013). Non-cell autonomous control of apoptosis by ligand-independent Hedgehog signaling in *Drosophila*. *Cell Death Differ* **20**, 302-11.
- Dent, L. G., Manning, S. A., Kroeger, B., Williams, A. M., Saiful Hilmi, A. J., Crea, L., Kondo, S., Horne-Badovinac, S. and Harvey, K. F.** (2019). The dPix-Git complex is essential to coordinate epithelial morphogenesis and regulate myosin during *Drosophila* egg chamber development. *PLoS Genet* **15**, e1008083.
- Grzeschik, N. A., Amin, N., Secombe, J., Brumby, A. M. and Richardson, H. E.** (2007). Abnormalities in cell proliferation and apico-basal cell polarity are separable in *Drosophila* lgl mutant clones in the developing eye. *Dev Biol* **311**, 106-23.
- Grzeschik, N. A., Parsons, L. M., Allott, M. L., Harvey, K. F. and Richardson, H. E.** (2010). Lgl, aPKC, and Crumbs regulate the Salvador/Warts/Hippo pathway through two distinct mechanisms. *Curr Biol* **20**, 573-81.
- Kramatschek, B. and Campos-Ortega, J. A.** (1994). Neuroectodermal transcription of the *Drosophila* neurogenic genes *E(spl)* and *HLH-m5* is regulated by proneural genes. *Development* **120**, 815-26.
- Pennetta, G., Hiesinger, P. R., Fabian-Fine, R., Meinertzhagen, I. A. and Bellen, H. J.** (2002). *Drosophila* VAP-33A directs bouton formation at neuromuscular junctions in a dosage-dependent manner. *Neuron* **35**, 291-306.
- Petzoldt, A. G., Gleixner, E. M., Fumagalli, A., Vaccari, T. and Simons, M.** (2013). Elevated expression of the V-ATPase C subunit triggers JNK-dependent cell invasion and overgrowth in a *Drosophila* epithelium. *Dis Model Mech* **6**, 689-700.
- Pojer, J. M., Manning, S. A., Kroeger, B., Kondo, S. and Harvey, K. F.** (2021). The Hippo pathway uses different machinery to control cell fate and organ size. *iScience* **24**, 102830.
- Vaccari, T., Duchi, S., Cortese, K., Tacchetti, C. and Bilder, D.** (2010). The vacuolar ATPase is required for physiological as well as pathological activation of the Notch receptor. *Development* **137**, 1825-32.
- Venken, K. J., Schulze, K. L., Haelterman, N. A., Pan, H., He, Y., Evans-Holm, M., Carlson, J. W., Levis, R. W., Spradling, A. C., Hoskins, R. A. et al.** (2011). MiMIC: a highly versatile transposon insertion resource for engineering *Drosophila melanogaster* genes. *Nat Methods* **8**, 737-43.
- Wang, Y., Zhang, H., Shi, M., Liou, Y. C., Lu, L. and Yu, F.** (2017). Sec71 functions as a GEF for the small GTPase Arf1 to govern dendrite pruning of *Drosophila* sensory neurons. *Development* **144**, 1851-1862.